Finite Volume Schemes on Unstructured Grids for Non-Local Models: Application to the Simulation of Heat Transport in Plasmas

Thierry Goudon[a,*], Martin Parisot[b]

[a] *Team COFFEE, INRIA Sophia Antipolis Mediterranée*
& Labo. J. A. Dieudonné CNRS-Univ. Nice Sophia Antipolis (UMR 7351)
Parc Valrose 06108 Nice cedex 02, France
[b] *Project-Team SIMPAF-INRIA Lille Nord Europe*
Park Plazza, 40 avenue Halley F-59650 Villeneuve d'Ascq cedex, France

Abstract

In the so-called Spitzer-Härm regime, equations of plasma physics reduce to a non linear parabolic equation for the electronic temperature. Coming back to the derivation of this limiting equation through hydrodynamic regime arguments, one is led to construct a hierarchy of models where the heat fluxes are defined through a non-local relation which can be reinterpreted as well by introducing coupled diffusion equations. We address the question of designing numerical methods to simulate these equations. The basic requirement for the scheme is to be asymptotically consistent with the Spitzer-Härm regime. Furthermore, the constraints of physically realistic simulations make the use of unstructured meshes unavoidable. We develop a Finite Volume scheme, based on Vertex-Based discretization, which reaches these objectives. We discuss on numerical grounds the efficiency of the method, and the ability of the generalized models in capturing relevant phenomena missed by the asymptotic problem.

Keywords: Plasma physics, Non-local models, Finite Volume Method, Unstructured Meshes.
2000 MSC: 82D10 76M12 65M08 82C70

1. Introduction

The evolution of a plasma can be described by the Vlasov-Maxwell-Fokker-Planck system which is a set of coupled PDEs satisfied by the phase space distribution of charged particles and the electromagnetic fields. The numerical simulation of such a system is highly challenging. Sources of numerical difficulties are related on the one hand to the high dimensionality of the unknowns, and on the other hand to the presence of stiff terms in many situations of practical interest. Indeed, working with distributions of particles in phase space means that the unknown depends not only on time and space variables, but also on the velocity variable. Discretizing this additional variable and the corresponding (differential and integral) operators increases the size of the numerical unknowns. Next, from the physical properties of the plasma a set of dimensionless parameters can be defined, which govern the stability of the simulation. In many situations, like for instance for the simulation of ICF devices which has motivated the present work, the stiffness induced by the values of the parameters can be highly demanding in numerical resources and computational time. However, based on specific behavior of the parameters and using asymptotic arguments, we can find reduced models. In particular when the particles' distribution functions are driven

*Corresponding author
Email addresses: thierry.goudon@inria.fr (Thierry Goudon), martin.parisot@gmail.com (Martin Parisot)

to equilibrium (for instance due to the collisions mechanisms) we are led to models where the unknowns depend only on the time and space variables. The Spitzer-Härm regime discussed in the seminal work [1] is one of those regimes. We refer to [2, 3] for a detailed presentation of the scaling issues from the framework of kinetic equations. The asymptotic regime we are considering in this work combines two distinct effects:

- on the one hand, the small Debye length assumption leads to quasineutrality. The total current vanishes, and the local density of positive and negative charges equilibrate. Throughout the paper, we shall assume that the positive charges are in a given equilibrium state, with $u = 0$ as bulk velocity. Therefore the electronic current vanishes: denoting by $J(t, X)$ the first order moment of the electron distribution function, we have
$$J = 0. \tag{1.1}$$
This constraint is often used in practice, even in kinetic models; it defines self–consistently the electric field, see e. g. [4, 5, 6, 7]. More elaborate models can be considered, possibly incorporating a description of the fluctuations of the magnetic field [4, 8], but such refinements are beyond the scope of the present work.

- on the other hand, small values of the mean free path introduce relaxation effects, which, in turn, prescribe how the particles distribution function depends, at leading order, on the velocity variable. For our purposes, the asymptotic discussion is embodied into a single parameter, that we denote from now on by $0 < \varepsilon \ll 1$. The parameter ε is the ratio between the mean free path ℓ and the characteristic length of the considered flow L, see [2], i.e.
$$\varepsilon = \frac{\ell}{L} = \frac{\left(\varepsilon_0 k_B \bar{\theta} L\right)^2}{4\pi \bar{\rho} q^4 \ln \Lambda},$$
where ε_0 is the vacuum permittivity, k_B, the Boltzmann constant, q, the elementary charge and $\ln \Lambda$ the Coulomb logarithm, while $\bar{\rho}$ and $\bar{\theta}$ stand for typical values of the electronic density and temperature, respectively. This parameter measures the plasma thermalization.

It turns out that as ε goes to 0 the distribution of negative charges tends to a the local equilibrium and the dynamics of the plasma is entirely described by the evolution of the electron temperature $\theta(t, X)$ which obeys
$$\begin{cases} \partial_t \theta + \dfrac{2}{3\rho} \nabla_X \cdot Q = S, \\ Q = -\kappa_{SH}(\theta) \nabla_X \theta. \end{cases} \tag{1.2}$$
In (1.2), $X \mapsto \rho(X) > 0$ and $S(t, X)$ are God-given density and source term respectively. The diffusion coefficient $\theta \mapsto \kappa_{SH}(\theta) > 0$ keeps track of the microscopic description since its expression depends on the details of the interparticles collisions. The scaling issues and the derivation of (1.2) from the kinetic framework are detailed in [2, 3], which also contains further references.

Of course the limiting equation (1.2) is quite simple, and it can be solved numerically by using many efficient methods. However, it turns out that it misses some phenomena that should be inherited form the kinetic modeling, as it has been reported from comparizon with experiments or (1D or 2D) kinetic simulations [9, 10, 4]. Indeed, as ε increases, the influence of the deviation of the distribution from the equilibrium Maxwellian state become significant. Therefore, the objective consists in incorporating in the model some $\varepsilon-$dependent correction terms, intended to capture the effects of these deviations, but bearing in mind that the model should remain accessible to a reasonably costly numerical treatment. To this end,

models based on "delocalized heat fluxes" have been proposed in the literature since the pioneering work of Luciani, Mora and Virmont [11], see [12, 13, 14, 15]. The simplest non local models for heat transfer add a correction, defined by a suitable convolution kernel, to the definition of the heat flux in (1.2): we set $Q = -\kappa_{SH}(\theta)\nabla_X\theta + W_\varepsilon \star (\kappa_{SH}(\theta)\nabla_X\theta)$. The correction is intended to vanish as $\varepsilon \to 0$, and there are many derivations of relevant kernels W_ε [12, 13, 14, 15, 16, 5, 2]. For such simple models, usually the numerical treatment relies on IMEX approaches, the leading term being approached implicitly, the correction explicitly [16, 5]. We also refer to [2] for the mathematical analysis of such models. However, more refined reduced models have been proposed, which involve generalized heat fluxes depending on an energy variable [15].

The derivation of such non-local models has been revisited recently in [3] where the following system has been introduced as an alternative to the Spitzer-Härm equation:

$$\begin{cases} \partial_t\theta + \dfrac{2}{3\rho}\nabla_X \cdot Q = S, \\ Q(t,X) = \displaystyle\int_0^\infty \mathcal{Q}(t,X,\xi)\,\mathrm{d}\xi, \\ \partial_t\mathcal{Q} + \dfrac{\mathcal{Q}}{\varepsilon^2\mu} - \nabla_X\left(\nu\nabla_X\cdot\mathcal{Q}\right) - \eta\mathcal{E} = -\dfrac{\kappa}{\varepsilon^2\mu}\nabla_X\theta. \end{cases} \tag{1.3}$$

The additional variable $\xi \geq 0$ can be interpreted as an internal energy and $\mathcal{Q}(t,X,\xi)$ appears as to be a generalized heat flux, as already introduced by Schurtz and Nicolaï in [15]. The coefficients μ, ν, κ, η depend on both the energy variable ξ and the temperature θ, hence making the model non-linear (but they are supposed independent on the scaling parameter ε). Their expressions again depend on the collision processes; for our purposes, it is important to keep in mind that

$$\mu(\xi,\theta) > 0, \qquad \nu(\xi,\theta) > 0, \qquad \kappa(\xi,\theta) \in \mathbb{R}, \qquad \eta(\xi,\theta) \in \mathbb{R}$$

holds. It is convenient to define the electric field as

$$E = E_{SH} + \varepsilon^2\mathcal{E}, \qquad E_{SH} = \theta\left(\nabla_X \ln\rho - \frac{5}{2}\nabla_X\ln\theta\right),$$

and the perturbation $\mathcal{E}$ is defined in connection to the constraint (1.1), which now takes the form (see [3] for details)

$$J(t,X) = \frac{1}{\theta}\int_0^\infty \frac{\mathcal{Q}(t,X,\xi)}{\xi}\,\mathrm{d}\xi = 0. \tag{1.4}$$

The problem (1.3)-(1.4) is completed with the initial condition

$$\theta(0,X) = \theta^0(X), \qquad \mathcal{Q}(0,X,\xi) = \mathcal{Q}^0(X,\xi), \tag{1.5}$$

where $\mathcal{Q}^0(X,\xi)$ is assumed to satisfy the constraint (1.4). The problem is set on a smooth bounded domain Ω; on the boundary $\partial\Omega$ it is natural to use the Neumann condition

$$\mathcal{Q}(t,X,\xi)\cdot n_{\partial\Omega} = 0, \tag{1.6}$$

with $n_{\partial\Omega}$ the unit outward normal. As ε goes to 0, we formally recover (1.2), endowed with Neumann boundary condition, from (1.3), once we have said that

$$\kappa_{SH}(\theta) = \int_0^\infty \kappa(\xi,\theta)\,\mathrm{d}\xi > 0.$$

We point out that the integral is positive while $\kappa(\xi,\theta)$ changes sign so that (1.4) can be satisfied at the asymptotic regime $\varepsilon \to 0$. Remarkable properties of the model (1.3) are discussed in [3]. As a matter of fact, we observe that the total thermal energy $\int_\Omega 3\rho\theta \,\mathrm{d}X$ satisfies the following balance relation:

$$\frac{\mathrm{d}}{\mathrm{d}t}\int_\Omega 3\rho\theta \,\mathrm{d}X = \int_\Omega 3\rho S \,\mathrm{d}X. \tag{1.7}$$

As said above, throughout this paper we assume that quasineutrality holds with a ionic background without current: the electronic current vanishes (1.1) and the electronic density is prescribed. The constraint also defines the electric field perturbation. The model can be generalized in order to describe more complex electromagnetic behaviors. For instance the expression of the Spitzer-Härm electric field can be replaced by Ohm's law and the perturbation $\mathcal{E}$ is obtained through a constraint $J = J_i \neq 0$. Note however that the coefficients μ, ν, κ and η are functions of the electric field and their expression depend on the electric model. It is also possible to deal with more complex electric models, like Poisson's law, with additional equations to compute the electronic density. The derivation of the model in [3] does not consider the effects of the magnetic field, which would need to go back to the Maxwell system. Such an extension requires to define an adapted basis to decompose the electron distribution function, as introduced in [17]. Such models based on a more intricate physics are beyond the scope of the present work, where we focus on the design of specific numerical methods to solve (1.3). For discussion of non local models with magnetic fields, we refer to [4, 5, 6, 7]. It is also worth pointing out that, while these non–local models of heat transfer are quite popular in the modeling of laser produced plasmas, their applications to tokamaks' plasmas has also been discussed [18, 19].

The system (1.3) is not strictly of macroscopic type because it still involves the internal energy variable $\xi \geq 0$. The approach devised in [3] consists in replacing the continuous equations (1.3) by a discrete version where the generalized heat flux is evaluated at a reduced set of quadrature points $\xi_1, ..., \xi_g$, for some $g \in \mathbb{N} \setminus \{0\}$. This is motivated by the fact that the important quantities are defined by integrals of the generalized heat flux. To be more specific, we use a Gauss-Laguerre quadrature approximation : given $\alpha > -1$, and $g \in \mathbb{N} \setminus \{0\}$, we set $\xi_1, ..., \xi_g$ as to be the zeroes of the gth Laguerre generalized polynomials:

$$\mathscr{L}_g^{(\alpha)}(\xi) = \sum_{j=1}^{g} (-1)^j \binom{g+\alpha}{g-j} \frac{\xi^j}{j!}$$

For any smooth function $\xi \mapsto \mathcal{Q}(\xi)$ the following Gaussian quadrature formula

$$\int_0^\infty \mathcal{Q}(\xi)\,\mathrm{d}\xi = \sum_{j=1}^{g} \omega_j \mathcal{Q}(\xi_j) + \frac{g!\Gamma(g+\alpha+1)}{(2g)!}\partial_\xi^{2g}\left(\mathcal{Q}(\xi)\frac{e^\xi}{\xi^\alpha}\right)(c),$$

holds for some $c \geq 0$ where the weight ω_j is associated to ξ_j by

$$\omega_j = \frac{\Gamma(g+\alpha)\xi_j}{g!(g+\alpha)\left(\mathscr{L}_{g-1}^{(\alpha)}(\xi_j)\right)^2}\frac{e^{\xi_j}}{\xi_j^\alpha}.$$

We obtain now a purely macroscopic model by introducing $\mathcal{Q}_1(t,X),...,\mathcal{Q}_g(t,X)$, intended to be approximation of $\mathcal{Q}(t,X,\cdot)$ at the quadrature points $\xi_1,...,\xi_g$. The discrete model obtained that way reads

$$\begin{cases} \partial_t \theta + \dfrac{2}{3\rho}\nabla_X \cdot Q = S, \\ Q = \displaystyle\sum_{j=1}^{g} \omega_j \mathcal{Q}_j, \\ \partial_t \mathcal{Q}_j + \dfrac{\mathcal{Q}_j}{\varepsilon^2 \mu_j} - \nabla_X \left(\nu_j \nabla_X \cdot \mathcal{Q}_j\right) - \eta_j \mathcal{E} = -\dfrac{\kappa_j}{\varepsilon^2 \mu_j}\nabla_X \theta, \end{cases} \tag{1.8}$$

where the coefficients are simply given by evaluating the original coefficients at the quadrature points:

$$\mu_j(\theta) = \mu(\xi_j,\theta), \qquad \nu_j(\theta) = \nu(\xi_j,\theta), \qquad \kappa_j(\theta) = \kappa(\xi_j,\theta).$$

The constraint (1.4) becomes

$$\sum_{j=1}^{g} \frac{\omega_j \mathcal{Q}_j}{\xi_j} = 0. \tag{1.9}$$

For the boundary condition, we get

$$\mathcal{Q}_j \cdot n_{\partial\Omega} = 0. \tag{1.10}$$

By contrast to other non local models where usually fluxes are solutions of stationary equations, like for instance the Shurtz-Nicolaï system, (1.8) do not need any artificial and unphysical cut-off of the coefficients to cure the observed numerical instabilities [16, 5]. Furthermore, [3] establishes well-posedness and stability estimates statements which provide a rigorous basis to the model. Hence, (1.8) can be a valuable alternative to delocalized models in plasmas simulations. As a first attempt a numerical scheme on Cartesian grids is proposed in [3], which allows to validate the relevancy of the reduced model. However, most applications need more elaborate discretizations based on unstructured meshes, because of complex geometries, mesh refinement strategies or coupling of the plasma equations with other physical effects. For this reason, we shall design a specific scheme based on a Finite Volume discretization, which can work on unstructured tessellations.

Let us describe how our work takes place in a more ambitious program. To perform simulation of ICF devices at the industrial level, the dynamic of ions has to be considered. Heating processes lead to expansion of the plasma and, at the hydrodynamic scale, such phenomena are usually simulated by using Lagrangian methods, hence with distorted meshes, see for instance [20, 21]. The work–plan to solve the coupled ions-electrons system splits into two steps, assuming for the sake of simplicity thermal equilibrium between positive and negative charges:

a) For a given ionic temperature, the dynamic of ions is computed on a unstructured grid by using a Lagrangian method on a "coarse" time step.

b) According to the quasi-neutrality assumption, the electronic density is set equal to the ionic density. It supposes that the electronic density does not vary too much on the "coarse" time step. Then, we update the electronic temperature: we perform several "fine" time steps by using the model (1.3) until we reach the "coarse" time step. We refer to [22] and the references therein for comments and analysis on such "sub–cycling" strategies. Eventually, we close the system by considering that the ionic temperature is equal to the electronic temperature.

In this program it might be questionable to make use of the quasineutrality assumption in order to impose the electronic density with the density of ions, which itself is driven by an hydrodynamic system. However,

this assumption is currently used in simulations of ICF devices, see [5]; it can be motivated by the fact the evolution of the electrons is widely faster than the evolution of the ions, see [2]. Note also that volume variations associated to the plasma expansion are described by source terms in the temperature equation. The actual expression of those source terms, describing the heating processes in the temperature equation, involves the electron distribution function F. According to the derivation and analysis in [3], we are able to reconstruct an approximation of the electron distribution with the solution of the macroscopic model (1.8). More precisely, given Ω in the unit sphere, we set

$$F\left(t,X,\xi\Omega\right)=M\left(t,X,\xi\right)+\varepsilon f_1\left(t,X,\xi\right)\cdot\Omega+\varepsilon^2\widetilde{f}_0\left(t,X,\xi\right),$$

where the deviation from the Maxwellian

$$M(t,X,\xi)=\frac{\rho(X)}{\left(2\pi\theta(t,X)\right)^{3/2}}e^{-\xi}$$

is defined by

$$\begin{aligned}
&f_1(t,X,\xi)=\frac{3\mathcal{Q}(t,X,\xi)}{16\pi\theta(t,X)^3\xi^2},\\
&\widetilde{f}_0(t,X,\xi)=-\frac{2\tau_0}{3}\left(\frac{\sqrt{2\theta(t,X)\xi}}{2}\,\nabla_x\cdot f_1(t,X,\xi)+\frac{E_0(t,X)}{\sqrt{2\theta(t,X)\xi}}\cdot f_1(t,X,\xi)\right),\\
&E_0(t,X)=\theta\left(\nabla_X\ln\rho+\frac{5}{2}\nabla_X\ln\theta\right)(t,X),
\end{aligned}$$

with $\tau_1>0$ and $\tau_2>0$. We have adopted here the simplifying assumptions described in [3, §5.1, simplifications b) and c)], which have been used to derive (1.3). Such a formula provides an expression of the source term. However, it is likely that the simplifications which lead to a practical formula introduce a gap with the real physical process of heating. The interpretation of the results could be challenging, and it could be far from easy to distinguish whether discrepancies with observations are due to inabilities of the numerical method of weaknesses of the adopted reduced model. Another source term in the generalized heat flux equation is related to the heating process by the inverse bremsstrahlung effect induced by the beam. To simulate physical devices, another critical data that must be provided in the numerical models are the boundary conditions. However, measurements of the internal energy profile of the electronic distribution are not available, and thus it is not clear how to define a boundary condition for the non-local models.

This work focuses on part b) of the program. We suppose that the density and the source term are given and we pay attention to the numerical resolution on quite arbitrary grids of the generalized heat flux equation. We propose a scheme of Finite Volume type to perform simulation of the system (1.8)-(1.10). Of course numerical schemes for the Spitzer-Härm equation (1.2) are quite standard, so that a natural requirement is to construct the scheme for (1.8)-(1.10) in such a way it degenerates as $\varepsilon\to 0$ to one of those simple schemes for (1.2). A difficulty consists in avoiding unnecessary spreading of the numerical stencil: proceeding naively would lead to update fluxes and temperature at a given point by using a large number of neighbors. In turn, it would increase the complexity of the underlying linear system and thus would impact negatively the numerical efficiency, creating also spurious diffusion effects and ambiguities for treating boundary terms. The method has also some flexibility and it can be readily adapted to treat similar problems like the simulation of electrostatic potentials as arising in the modeling of the dielectric properties of water [23, 24]. We remind that usually numerical methods for non local models are designed

for systems where the heat fluxes are defined by stationary equations, which thus leads to different techniques. For such stationary models, stability issues usually leads to impose an artificial cut–off in the definition of the coefficients, which is however unphysical (in particular it contradicts the null–current hypothesis). We refer for details on such numerical schemes, mainly based on Finite Differences approaches, to [16, 5]. Further validation of the model and the scheme can be discussed through comparizon with experiments or kinetic simulations [25]. Performing microscopic codes are available even in 2D: we refer for instance to [26, 27] for a detailed presentation of numerical methods (on Cartesian grids) for solving kinetic models in a similar physical context.

The paper is organized as follows. In section 2, we use a simple time discretization and define a relevant space discretization which allows to reach our objectives. From a mesh made of triangles, the temperature is evaluated at the vertices of the meshing (Vertex Based Method) while the heat fluxes are evaluated on the interfaces of the corresponding control volumes. In this construction gradients are simply approximated by using $\mathbb{P}_1$ interpolations in triangles. In section 3, we present a coupling strategy which allows to use the Spitzer-Härm limit in a part of the computational domain and the generalized Spitzer-Härm model everywhere else. We are able to couple the models thanks to the consistency of the generalized Spitzer-Härm scheme to the Spitzer-Härm scheme. Section 4 is devoted to a series of numerical tests which bring out the numerical performances of the scheme and show the ability of the model (1.8)-(1.10) in capturing new effects. A more elaborate time discretization is discussed in Section 5.2: by using an iterative procedure, which is reminiscient of the Jacobi method, we uncouple the resolution of the heat fluxes equation, which substantially improves the performances of the scheme in terms of computational time.

2. A Vertex-Based Finite Volume Scheme

2.1. Discretization

2.1.1. Time Discretization

To start with let us discuss the time discretization. Let $h_t > 0$ denote the time step. Integrating

$$\partial_t \theta + \frac{2}{3\rho} \nabla_X \cdot Q = S, \qquad Q = \sum_{j=1}^{g} \omega_j \mathcal{Q}_j(t, X) \tag{2.1}$$

over $[nh_t, (n+1)h_t]$ we obtain

$$\theta((n+1)h_t, X) - \theta(nh_t, X) = \int_{nh_t}^{(n+1)h_t} S(t, X)\, \mathrm{d}t - \frac{2}{3\rho} \nabla_X \cdot \sum_{j=1}^{g} \omega_j \int_{nh_t}^{(n+1)h_t} \mathcal{Q}_j \, \mathrm{d}t.$$

The source term S is known, and we denote

$$S^{n,n+1}(X) = \frac{1}{h_t} \int_{nh_t}^{(n+1)h_t} S(t, X)\, \mathrm{d}t.$$

For the fluxes the integral $\int_{nh_t}^{(n+1)h_t} \mathcal{Q}_j \, \mathrm{d}t$ is approximated by interpolating between the values of $\mathcal{Q}_j$ at time nh_t and $(n+1)h_t$. Given a parameter $0 \leq \tau \leq 1$, we are thus led to the following semi-discrete version of (2.1)

$$\frac{\theta^{n+1} - \theta^n}{h_t} = S^{n,n+1} - \frac{2}{3\rho} \nabla_X \cdot \sum_{j=1}^{g} \omega_j (\tau \mathcal{Q}_j^{n+1} + (1-\tau) \mathcal{Q}_j^n). \tag{2.2}$$

Proceeding similarly with the fluxes equations yields

$$\begin{aligned}\frac{\mathcal{Q}_j^{n+1}-\mathcal{Q}_j^n}{h_t}+\frac{\tau\mathcal{Q}_j^{n+1}+(1-\tau)\,\mathcal{Q}_j^n}{\varepsilon^2\mu_j^{n+\tau}}-\nabla_X\left(\nu_j^{n+\tau}\nabla_X\cdot\left(\tau\mathcal{Q}_j^{n+1}+(1-\tau)\,\mathcal{Q}_j^n\right)\right)\\ -\eta_j^{n+\tau}\left(\tau\mathcal{E}^{n+1}+(1-\tau)\,\mathcal{E}^n\right)=-\frac{\kappa_j^{n+\tau}}{\varepsilon^2\mu_j^{n+\tau}}\nabla_X\left(\tau\theta^{n+1}+(1-\tau)\,\theta^n\right).\end{aligned}\tag{2.3}$$

The coefficients are defined by

$$\begin{aligned}\mu_j^{n+\tau}&=\mu_j\left(\tau\theta^{n+1}+(1-\tau)\,\theta^n\right)\\ \nu_j^{n+\tau}&=\nu_j\left(\tau\theta^{n+1}+(1-\tau)\,\theta^n\right),\\ \kappa_j^{n+\tau}&=\kappa_j\left(\tau\theta^{n+1}+(1-\tau)\,\theta^n\right).\end{aligned}$$

The field $\mathcal{E}^n$ is defined as to maintain the constraint

$$\sum_{j=1}^{g}\frac{\omega_j\mathcal{Q}_j^n}{\xi_j}=0.\tag{2.4}$$

In the following, we shall use the shorthand notation

$$\theta^{n+\tau}=\tau\theta^{n+1}+(1-\tau)\,\theta^n,\quad \mathcal{Q}_j^{n+\tau}=\tau\mathcal{Q}_j^{n+1}+(1-\tau)\,\mathcal{Q}_j^n,\quad \mathcal{E}^{n+\tau}=\tau\mathcal{E}^{n+1}+(1-\tau)\,\mathcal{E}^n.$$

It can be interpreted as an approximation of the corresponding unknowns at time $(n+\tau)\,h_t$. The parameter τ allows to tune how much the scheme is made implicit, in connection to stability and accuracy issues. As $\tau=0$, the scheme is fully explicit. But, according to the analysis in [2] it is likely that the stability of the scheme is constrained by a condition of parabolic type, where the time step have to be in order of the square of the space step, which makes the computational cost prohibitive, especially for multi-dimensional simulations. Hence, using $0<\tau\leq 1$ makes the scheme implicit and improves the stability properties. However, due to the fact that the coefficients depend on θ, the system (2.2)-(2.4) is non linear for $\tau>0$.

To deal with the nonlinearities, we proceed iteratively. Knowing the unknowns at time nh_t, we construct a sequence $\left(\theta^{n,r},\mathcal{Q}_1^{n,r},...,\mathcal{Q}_g^{n,r}\right)_{r\in\mathbb{N}}$ the limit of which as $r\to\infty$ will define θ^{n+1} and the $\mathcal{Q}_j^{n+1}$'s. We set $\theta^{n,0}=\theta^n$, $\mathcal{Q}_j^{n,0}=\mathcal{Q}_j^n$ and we define iteratively $\theta^{n,r}$ and $\mathcal{Q}_1^{n+\tau,r},...,\mathcal{Q}_g^{n+\tau,r}$ by solving the linear system

$$\begin{cases}\mathcal{Q}_j^{n+\tau,r+1}-\varepsilon^2\tilde{\mu}_j^{n+\tau,r}\nabla_X\left(\nu_j^{n+\tau,r}\nabla_X\cdot\mathcal{Q}_j^{n+\tau,r+1}\right)-\dfrac{2}{3}\tilde{\kappa}_j^{n+\tau,r}\tau h_t\nabla_X\left(\dfrac{1}{\rho}\nabla_X\cdot\displaystyle\sum_{l=1}^{g}\omega_l\mathcal{Q}_l^{n+\tau,r+1}\right)\\ \qquad-\varepsilon^2\tilde{\mu}_j^{n+\tau,r}\eta_j^{n+\tau,r}\mathcal{E}^{n+\tau,r+1}=\dfrac{\varepsilon^2\tilde{\mu}_j^{n+\tau,r}}{\tau h_t}\mathcal{Q}_j^n-\tilde{\kappa}_j^{n+\tau,r}\nabla_X\left(\theta^n+\tau h_t S^{n,n+1}\right)\\ \displaystyle\sum_{j=1}^{g}\frac{\omega_j\mathcal{Q}_j^{n+\tau,r+1}}{\xi_j}=0,\end{cases}\tag{2.5}$$

$$\theta^{n+\tau,r+1}=\theta^n+\tau h_t S^{n,n+1}-\frac{2\tau h_t}{3\rho}\nabla_X\cdot\sum_{j=1}^{g}\omega_j\mathcal{Q}_j^{n+\tau,r+1},$$

where we have set

$$\begin{aligned}
&\mu_j^{n+\tau,r}(\theta) = \mu_j\left(\theta^{n+\tau,r}\right), \qquad && \tilde{\mu}_j^{n+\tau,r}(\theta) = \frac{\mu_j^{n+\tau,r}(\theta)\,\tau h_t}{\varepsilon^2 \mu_j^{n+\tau,r}(\theta) + \tau h_t},\\
&\nu_j^{n+\tau,r}(\theta) = \nu_j\left(\theta^{n+\tau,r}\right),\\
&\eta_j^{n+\tau,r}(\theta) = \eta_j\left(\theta^{n+\tau,r}\right),\\
&\kappa_j^{n+\tau,r}(\theta) = \kappa_j\left(\theta^{n+\tau,r}\right), \qquad && \tilde{\kappa}_j^{n+\tau,r}(\theta) = \frac{\kappa_j^{n+\tau,r}(\theta)\,\tau h_t}{\varepsilon^2 \mu_j^{n+\tau,r}(\theta) + \tau h_t}.
\end{aligned} \tag{2.6}$$

In practice, a few iterations are sufficent to obtain a good approximation of the limit of the iterative process. We are thus led to solve a system of elliptic equations and we are going to discuss in the following section the space discretization of (2.5) based on a Finite Volume formulation of the problem.

2.1.2. Finite Volume Discretization

For the sake of simplicity, we restrict the presentation to the two-dimension framework. We give some hints for the generalization to the 3D case in Section 5.1 below. Since solutions of (1.3) are expected to converge to those of (1.2) in the Spitzer-Härm regime $\varepsilon \to 0$, we start by writing a scheme for the limit equation.

We can rewrite the problem as a single equation for the temperature θ

$$3\rho\partial_t\theta - 2\nabla_X \cdot (\kappa_{SH}\nabla_X\theta) = S \tag{2.7}$$

According to the discussion in Section 2.1.1, we are led to consider the following semi-discrete problem

$$\theta^{n+\tau,r+1} - \frac{2\tau h_t}{3\rho}\nabla_X \cdot \left(\kappa_{SH}^{n+\tau,r}\nabla_X\left(\theta^{n+\tau,r+1}\right)\right) = \theta^n + \tau h_t S^{n,n+1}, \tag{2.8}$$

with $\kappa_{SH}^{n+\tau,r} = \sum_{j=1}^{g}\kappa_j^{n+\tau,r}$. Adopting the Finite Volume viewpoint, the numerical unknown will be intended to approximate the mean value of the temperature over some control volume, and we will need to introduce a suitable definition of the gradient of the temperature on the interfaces of the control volume.

In this work we consider a tessellation of the computational domain Ω , noted $\mathbb{T}$, made of conforming and isotropic triangles. It constitutes the so-called primal mesh.The temperature is estimated at the vertices of the mesh. We denote by $\mathbb{V}$ the set of vertices of the tessellation $\mathbb{T}$, and $\mathscr{C}_k$ the control volume associated to the vertex $k \in \mathbb{V}$. As shown in Figure (1), it is obtained by joining the centroids of all the triangles having k as a vertex and the midpoint of the edges of these triangles. The segments of this polygonal curve containing $\mathscr{C}_k$ are called the faces of the control volume, and $|\mathscr{C}_k| = \int_{\mathscr{C}_k} \mathrm{d}X$ stands for the surface (volume in dimension 3) of the domain $\mathscr{C}_k$. The set of the control volumes defines another tessellation of Ω, named the dual mesh. Finally, we denote by $\mathbb{F}_{\mathscr{C}_k}$, the set of the faces of $\mathscr{C}_k$ which do not belong to $\partial\Omega$. Faces lying on $\partial\Omega$ can be disregarded due to the Neumann boundary condition (1.10).
Let us integrate (2.8) over a control volume $\mathscr{C}_k$. By using the Stokes formula, we obtain

$$\begin{aligned}
&\frac{1}{|\mathscr{C}_k|}\int_{\mathscr{C}_k}\rho\theta^{n+\tau,r+1}\,\mathrm{d}X - \frac{2\tau h_t}{3|\mathscr{C}_k|}\sum_{f\in\mathbb{F}_{\mathscr{C}_k}}\int_f\left(\kappa_{SH}^{n+\tau,r}\nabla_X\left(\theta^{n+\tau,r+1}\right)\right)\mathrm{d}\sigma\cdot\frac{N_{\mathscr{C}_k}^f}{|f|}\\
&\quad = \frac{1}{|\mathscr{C}_k|}\int_{\mathscr{C}_k}\rho\theta^n\,\mathrm{d}X + \tau h_t\frac{1}{|\mathscr{C}_k|}\int_{\mathscr{C}_k}\rho S^{n,n+1}\,\mathrm{d}X,
\end{aligned} \tag{2.9}$$

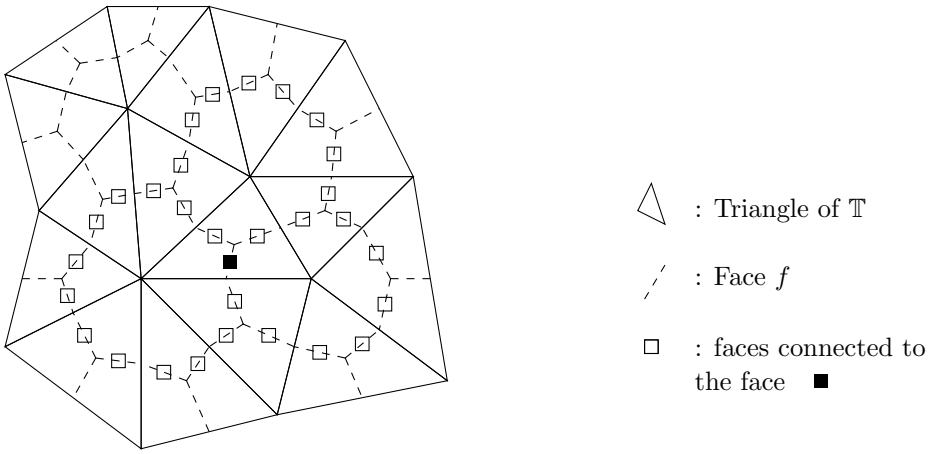

Figure 1: Example of control volume $\mathscr{C}_k$ and connectivity.

where $N^f_{\mathscr{C}_k}$ is the normal to the face f outward of the volume $\mathscr{C}_k$ with norm $|N^f_{\mathscr{C}_k}| = |f| = \int_f \mathrm{d}\sigma$, the length of the face. We set

$$\rho_k = \frac{1}{|\mathscr{C}_k|}\int_{\mathscr{C}_k} \rho \,\mathrm{d}X, \qquad S_k^{n,n+1} = \frac{1}{\rho_k|\mathscr{C}_k|}\int_{\mathscr{C}_k} \rho S^{n,n+1}\,\mathrm{d}X.$$

The numerical unknown $\theta_k^{n+\tau,r+1}$ is intended to approximate the mean value $\frac{1}{|\mathscr{C}_k|}\int_{\mathscr{C}_k}\theta^{n+\tau,r+1}\,\mathrm{d}X$. The scheme will be defined by mimicking relation (2.9). To this end we need to define the numerical flux on the faces of $\mathscr{C}_k$ which relies on constructing the gradient of the temperature on the faces. The idea consists is using the three vertices of the triangle containing the considered interface to define a $\mathbb{P}_1$ approximation of the temperature, then taking its derivative to obtain the gradient. Such a construction already appears in fluid mechanics when dealing with non homogeneous incompressible viscous flows [28]. It can be compared to DDFV construction which are usually based on Cell Center discretization see [29, 30] and the references therein. More precisely, the construction proceeds as follows. Let $K = \#\mathbb{V}$ be the cardinal of the set of vertices of the mesh. Given $\psi \in \mathbb{R}^K$, we set

$$\mathscr{P}[\psi](X) = \sum_{T\in\mathbb{T}}\left(\nabla_T[\psi]\cdot\left(X - \frac{\sum_{k\in\mathbb{V}_T} X_k}{3}\right) + C_T[\psi]\right)\mathbf{1}_T, \tag{2.10}$$

where $\mathbb{V}_T$ is the set of the vertices of the triangle T and X_k is the vector of coordinates of the vertex k. The definition is completed by imposing

$$\mathscr{P}[\psi](X_k) = \psi_k.$$

In other words we consider the piecewise $\mathbb{P}_1$ function having its values at the vertices prescribed by the ψ_k's. We have

$$(\nabla_T[\psi])_i = \frac{\det(W^i)}{\det(V)}, \qquad C_T[\psi] = \frac{\sum_{k\in\mathbb{V}_T}\psi_k}{3},$$

with V the 2×2 matrix with coefficients $V_{j,k} = (X_{l_k} - X_{l_3})_j$ while $(l_i)_{1\le i\le 3}$ are indices of vertices of triangle T. W^i is obtained from V by replacing its i^{th} column by the column vector $(\psi_{l_1} - \psi_{l_3}, \psi_{l_2} - \psi_{l_3})^t$.

The definition makes sense because $\det(V)$ vanishes iff the surface of T vanishes, and for a given mesh this quantity is bounded from below. Observe that $\mathscr{P}[\psi]$ is continuous on Ω. Going back to the numerical scheme, we write

$$\theta_k^{n+\tau,r+1} - \frac{2\tau h_t}{3\rho_k|\mathscr{C}_k|}\sum_{f\in\mathbb{F}_{\mathscr{C}_k}} \kappa_{SH,f}^{n+\tau,r}\nabla_{T_f}\left[\theta^{n+\tau,r+1}\right]\cdot N_{\mathscr{C}_k}^f = \theta_k^n + \tau h_t S_k^{n,n+1}, \tag{2.11}$$

where T_f is the triangle which contains the face f, $\kappa_{SH,f} = \kappa_{SH}^{n+\tau,r}\left(\mathscr{P}[\theta](X_f)\right)$ and X_f being the centroid of the face f.

We shall use the scheme just derived for (1.2) as a starting point to develop a numerical method for the more involved model (1.3). To this end, it is convenient to introduce the vectorial quantity, naturally associated to faces f of the control volumes,

$$Q_{SH,f}^{n+\tau,r+1} = -\kappa_{SH,f}^{n+\tau,r}\nabla_{T_f}\left[\theta^{n+\tau,r+1}\right]. \tag{2.12}$$

It can be interpreted as an approximation of the heat flux in the direction of the normal to the face f at time $(n+\tau)h_t$, that is

$$\frac{1}{|f|}\int_f Q_{SH}\left((n+\tau)h_t,\sigma\right)\,\mathrm{d}\sigma.$$

Remark that $\psi\in\mathbb{R}^K \mapsto \mathscr{P}[\psi]$ is a linear operator. We replace $\theta^{n+\tau,r+1}$ in (2.12) by the expression given in (2.11) to obtain

$$\begin{aligned} Q_{SH,f}^{n+\tau,r+1} - \frac{2\kappa_{SH,f}^{n+\tau,r}\tau h_t}{3}\nabla_{T_f}\left[\frac{1}{\rho|\mathscr{C}|}\sum_{f^\star\in\mathbb{F}_{\mathscr{C}_k}} Q_{SH,f^\star}^{n+\tau,r+1}\cdot N_{\mathscr{C}}^f\right] \\ = -\kappa_{SH,f}^{n+\tau,r}\nabla_{T_f}\left[\theta^n + \tau h_t S_k^{n,n+1}\right], \end{aligned} \tag{2.13}$$

$$\theta_k^{n+\tau,r+1} = \theta_k^n + \tau h_t S_k^{n,n+1} - \frac{2\tau h_t}{3\rho_k|\mathscr{C}_k|}\sum_{f\in\mathbb{F}_{\mathscr{C}_k}} Q_{SH,f}^{n+\tau,r+1}\cdot N_{\mathscr{C}_k}^f.$$

Obviously (2.13) defines the same sequence θ_k^n as (2.11). However, as a numerical scheme it is not relevant to make use of (2.13) because it involves more unknowns and the linear system to be inverted has a larger stencil and loses some advantageous proporties as symmetry, Figure (1). Nevertheless, formula (2.13) is interesting because it provides a natural way to evaluate the consistency of a scheme for (1.3) with the Spitzer-Härm regime $\varepsilon\to 0$: letting ε go to 0 in the definition of the flux for (1.3) we should recover (2.13). As already noticed, the heat flux in (2.12) is naturally discretized on the faces of the control volumes. Therefore, the new numerical unknown for (1.3) $\mathcal{Q}_{j,f}^{n+\tau,r+1}$ is interpreted as an approximation of the mean value of $\mathcal{Q}_j^{n+\tau,r+1}$ on the face f. Remark we do not associate a control volume to the discrete unknown $\mathcal{Q}_{j,f}^{n+\tau,r+1}$. However, we are able to define discrete second order differential operators on the generalized heat fluxes on the faces, need to the resolution of (1.3). To this end, we first remark that for any $Q:\mathbb{R}^2\to\mathbb{R}^2$ smooth enough vector function, the integration of the Jacobian matrix $\nabla_X Q$ on a bounded surface could be estimated using a Stokes formulae by its mean value on the boundary of the surface. In particular, on a control volume k, we have

$$\int_{\mathscr{C}_k}\nabla_X Q\,\mathrm{d}X = \int_{\partial\mathscr{C}_k} Q\otimes n\,\mathrm{d}\sigma = \sum_{f\in\mathbb{F}_{\mathscr{C}_k}}\frac{1}{|f|}\int_f Q\,\mathrm{d}\sigma\otimes N_{\mathscr{C}_k}^f,$$

with n the outward normal to the boundary $\partial\mathscr{C}_k$. Mimicking this formulae, we proceed into two steps.

1. Let $q = (q_1, ..., q_M)$ be a given set of M vectors in $\mathbb{R}^2$, with M the number of faces of the mesh. Hence each q_j is associated to a unique face of the dual mesh. We associate to q the piecewise constant matrix-valued function which is defined of each volume control by

$$\mathscr{G}_k[q] = \frac{1}{|\mathscr{C}_k|} \sum_{f \in \mathbb{F}_{\mathscr{C}_k}} q_f \otimes N^f_{\mathscr{C}_k}. \tag{2.14}$$

   This quantity is intended to define the (discrete) mean derivative of a function on a control volume from the values on the faces.
2. The previous step defines $\mathscr{G}_1[q], ..., \mathscr{G}_K[q]$, associating to each vertex k of the primal mesh. Then we can use the operator $\mathscr{P}$ to construct a function which is $\mathbb{P}_1$ on each triangle $T \in \mathbb{T}$ and next consider $\nabla_{T_f}[\mathscr{G}[q]]$ for each face of the dual mesh.

Coming back to the equations under consideration, Step 1 defines $\mathrm{Tr}\big(\mathscr{G}_k\left[\mathcal{Q}_j^{n+\tau,r+1}\right]\big)$: on each control volume $\mathscr{C}_k$, this quantity is intended to approximate $\frac{1}{|\mathscr{C}_k|}\int_{\mathscr{C}_k} \nabla_X \cdot \mathcal{Q}_j^{n+\tau,r+1}\,\mathrm{d}X$. Then using the reconstruction by triangle $\mathscr{P}$, we are able to define on each $T \in \mathbb{T}$ an approximation of the second order derivative of the generalized heat fluxes with $\nabla_T\left[\mathrm{Tr}\big(\mathscr{G}\left[\mathcal{Q}_j^{n+\tau,r+1}\right]\big)\right]$. With these notations, we arrive at the following definition of the scheme: for any face f we have

$$\begin{aligned}
&\mathcal{Q}_{j,f}^{n+\tau,r+1} - \varepsilon^2\tilde{\mu}_{j,f}^{n+\tau,r}\nabla_{T_f}\left[\nu_j^{n+\tau,r}\,\mathrm{Tr}\big(\mathscr{G}\left[\mathcal{Q}_j^{n+\tau,r+1}\right]\big)\right] \\
&\quad - \frac{2\tilde{\kappa}_{j,f}^{n+\tau,r}\tau h_t}{3}\nabla_{T_f}\left[\frac{1}{\rho}\,\mathrm{Tr}\left(\mathscr{G}\left[\sum_{l=1}^{g}\omega_l\mathcal{Q}_l^{n+\tau,r+1}\right]\right)\right] - \varepsilon^2\tilde{\mu}_{j,f}^{n+\tau,r}\eta_{j,f}^{n+\tau,r}\mathcal{E}_f^{n+\tau,r+1} \\
&\qquad = \frac{\varepsilon^2\tilde{\mu}_{j,f}^{n+\tau,r}}{\tau h_t}\mathcal{Q}_{j,f}^{n} - \tilde{\kappa}_{j,f}^{n+\tau,r}\nabla_{T_f}\left[\theta^n + \tau h_t S_k^{n,n+1}\right], \\
&\sum_{j=1}^{g}\frac{\omega_j\mathcal{Q}_{j,f}^{n+\tau,r+1}}{\xi_j} = 0,
\end{aligned} \tag{2.15}$$

and for $k \in \{1, ..., K\}$ we have

$$\theta_k^{n+\tau,r+1} = \theta_k^n + \tau h_t S_k^{n,n+1} - \frac{2\tau h_t}{3\rho_k}\,\mathrm{Tr}\left(\mathscr{G}_k\left[\sum_{j=1}^{g}\omega_j\mathcal{Q}_j^{n+\tau,r+1}\right]\right). \tag{2.16}$$

The coefficients are given by

$$\begin{aligned}
&\tilde{\mu}_{j,f}^{n+\tau,r} = \frac{1}{|f|}\int_f \tilde{\mu}_j^{n+\tau,r}\left(\mathscr{P}[\theta](X)\right)\mathrm{d}\sigma, \quad \tilde{\kappa}_{j,f}^{n+\tau,r} = \frac{1}{|f|}\int_f \tilde{\kappa}_j^{n+\tau,r}\left(\mathscr{P}[\theta](X)\right)\mathrm{d}\sigma, \\
&\eta_{j,f}^{n+\tau,r} = \frac{1}{|f|}\int_f \eta_j^{n+\tau,r}\left(\mathscr{P}[\theta](X)\right)\mathrm{d}\sigma, \quad \nu_{j,k}^{n+\tau,r} = \frac{1}{|\mathscr{C}_k|}\int_{\mathscr{C}_k}\nu_j^{n+\tau,r}(\theta_k)\,\mathrm{d}X = \nu_j^{n+\tau,r}(\theta_k).
\end{aligned} \tag{2.17}$$

The linear system (2.15) is the heart of the scheme; it is the main source of numerical cost because this is only step in the scheme which requires to solve a linear system. It is made of $g+1$ equations (generalized heat fluxes + constraint) and $g+1$ degrees of freedom (generalized heat fluxes + field perturbation) at each face. The perturbation of the electric field plays the role of the Lagrangian multiplier associated to

the constraint of vanishing current. It is incorporated in the linear system to be solved. Other methods could be used based on the optimization viewpoint : Uzawa algorithm, augmented Lagrangian methods... The method we use guarantees that the constraint is exactly satisfied, see [3]. The numerical resolution could be generalized to more intricate electromagnetic models, while the discretization of the electric field is realized at the faces. Remark that the Neumann boundary condition is naturally taken into account by imposing

$$\mathcal{Q}_{j,f}^{n+\tau,r+1} \cdot N_{\mathscr{C}_k}^f = 0 \quad \text{when } f \in \partial\Omega$$

and k is the index of the volume which admits f as a face. Accordingly, the boundary terms are also incorporated in the summation over the faces. We can check that the scheme satisfies the discrete analog of the energy balance relation (1.7).

Proposition 2.1. *The solution of the scheme* (2.15)-(2.16) *satisfies*

$$\sum_{k\in\mathbb{V}} 3|\mathscr{C}_k|\rho_k\theta_k^{n+1} = \sum_{k\in\mathbb{V}} 3|\mathscr{C}_k|\rho_k\theta_k^{n} + h_t \sum_{k\in\mathbb{V}} 3|\mathscr{C}_k|\rho_k S_k^{n,n+1}.$$

Proof. Let us replace the temperature by its expression given by (2.16). We write for any $r \geq 0$

$$\begin{aligned}\sum_{k\in\mathbb{V}} 3|\mathscr{C}_k|\rho_k\theta_k^{n,r+1} &= \sum_{k\in\mathbb{V}} 3|\mathscr{C}_k|\rho_k \left(\frac{1}{\tau}\left(\theta_k^n + \tau h_t S_k^{n,n+1} - \frac{2\tau h_t}{3\rho_k}\,\mathrm{Tr}\left(\mathscr{G}_k\left[\sum_{j=1}^{g}\omega_j \mathcal{Q}_j^{n+\tau,r+1}\right]\right)\right) - \frac{1-\tau}{\tau}\theta_k^n\right)\\ &= \sum_{k\in\mathbb{V}} 3|\mathscr{C}_k|\rho_k\theta_k^n + \sum_{k\in\mathbb{V}} 3|\mathscr{C}_k|\rho_k h_t S_k^{n,n+1} - 2h_t\sum_{j=1}^{g}\omega_j \sum_{k\in\mathbb{V}}\sum_{f\in\mathbb{F}_{\mathscr{C}_k}} \mathcal{Q}_{j,f}^{n+\tau,r+1}\cdot N_{\mathscr{C}_k}^f\end{aligned}$$

In the last sum, the contribution of the boundary faces vanishes owing to the Neumann boundary condition. Let us consider an internal face $f \cap \partial\Omega = \emptyset$, common to two control volumes $\mathscr{C}_{k_1}^f$ and $\mathscr{C}_{k_2}^f$. The outward normal of these control volumes on the face f are in opposite directions: $N_{\mathscr{C}_{k_1}}^f = -N_{\mathscr{C}_{k_2}}^f$. It follows that

$$\sum_{k\in\mathbb{V}}\sum_{f\in\mathbb{F}_{\mathscr{C}_k}} \mathcal{Q}_{j,f}^{n+\tau,r+1}\cdot N_{\mathscr{C}_k}^f = \sum_{f\in\mathbb{F}} \mathcal{Q}_{j,f}^{n+\tau,r+1}\cdot\left(N_{\mathscr{C}_{k_1}}^f + N_{\mathscr{C}_{k_2}}^f\right) = 0,$$

where $\mathbb{F}$ is the set of faces in the interior of Ω. Eventually we conclude by passing to the limit $r \to \infty$. ∎

Remark 2.1. *We observe that the quantity* $\mathrm{Tr}\big(\mathscr{G}\,[q]\,\big)$ *depends only on the inner products* $q_f \cdot N_{\mathscr{C}_k}^f$. *Precisely, we have*

$$\mathrm{Tr}\big(\mathscr{G}\,[q]\,\big)\big|_{\mathscr{C}_k} = \frac{1}{|\mathscr{C}_k|}\sum_{f\in\mathbb{F}_{\mathscr{C}_k}} q_f \cdot N_{\mathscr{C}_k}^f.$$

Therefore it appears clearly that $\mathcal{Q}_{j,f}^{n+\tau,r}\cdot N_{\mathscr{C}_k}^f$ *is the only relevant variable to be used in the numerical scheme* (2.15). *It means that the unknowns reduce to a scalar quantity associated to each vertex of the primal mesh and g scalar quantities associated to each face of the dual mesh.*
Moreover, it is worth pointing out that the strategy, with the operators $\mathscr{P}$ *and* $\mathscr{G}$, *can be used to treat more general non-local equations, involving more complicated second order derivatives of the heat fluxes, see [3]. For instance* $\nabla_X\cdot\nabla_X\mathcal{Q}_j^{n+\tau,r+1}$ *becomes in the scheme*

$$\mathrm{Tr}\big(\nabla_{T_f}\left(\mathscr{G}\left[\mathcal{Q}_j^{n+\tau,r+1}\right]\right)\big).$$

Let us discuss what the scheme (2.15)-(2.16) does when ε goes to 0. Formally we obtain

$$\begin{aligned}
&\mathcal{Q}_{j,f}^{n+\tau,r+1} - \frac{2\kappa_{j,f}^{n+\tau,r}\tau h_t}{3}\nabla_{T_f}\left[\frac{1}{\rho}\operatorname{Tr}\left(\mathscr{G}\left[\sum_{l=1}^{g}\omega_l\mathcal{Q}_l^{n+\tau,r+1}\right]\right)\right] \\
&\qquad = -\kappa_{j,f}^{n+\tau,r}\nabla_{T_f}\left[\theta^n + \tau h_t S_k^{n,n+1}\right], \\
&\theta_k^{n+\tau,r+1} = \theta_k^n + \tau h_t S_k^{n,n+1} - \frac{2\tau h_t}{3\rho_k}\operatorname{Tr}\left(\mathscr{G}\left[\sum_{j=1}^{g}\omega_j\mathcal{Q}_j^{n+\tau,r+1}\right]\right).
\end{aligned} \tag{2.18}$$

Since the operator $\mathscr{P}$ is linear, we can rewrite the first equation using the second and we get $\mathcal{Q}_{j,f}^{n+\tau,r+1} = -\kappa_{j,f}^{n+\tau,r}\nabla_{T_f}\left[\theta^{n+\tau,r+1}\right]$. Finally we replace $\mathcal{Q}_{j,f}^{n+\tau,r+1}$ in the equation for the temperature by its expression and we arrive at (2.11).

2.2. Schurtz-Nicolaï Model

The Schurtz-Nicolaï model has been introduced in [15] as a relevant simplified model for ICF simulation. It can be recovered from (1.3) by neglecting the time derivative and the perturbation $\mathcal{E}$ in the equation for the heat fluxes. Therefore, the Schurtz-Nicolaï model reads

$$\begin{cases}
\partial_t\theta + \dfrac{2}{3\rho}\nabla_X\cdot Q = S, \\
\mathcal{Q} - \varepsilon^2\mu\nabla_X\left(\nu\nabla_X\cdot\mathcal{Q}\right) = -\kappa\nabla_X\theta, \\
Q = \displaystyle\int_0^\infty \mathcal{Q}\,\mathrm{d}\xi.
\end{cases} \tag{2.19}$$

Remark that the constraint (1.4) is not satisfied anymore. Furthermore it has been noticed that negative values of the coefficient κ might lead to instabilities (which is not the case for the time evolution problem, as shown in [3]), see [14], [9, Section III]. However, (2.19) is widely used in ICF codes, usually at the price of truncating κ in order to keep positive values only [15, Section III.C]. The delocalized operator is simplified and it makes the divergence of the generalized heat flux appear. Hence it is convenient to introduce the new scalar quantity $\tilde{\theta}\,(t,x,\xi) = \nabla_X\cdot\mathcal{Q}(t,x,\xi)$. It can be interpreted as the contribution to the evolution of the temperature of the generalized heat flux with a given internal energy ξ. We obtain a closed system involving the new variable by applying the divergence operator to the generalized heat flux equation. We are led to the following 2×2 system:

$$\begin{cases}
\partial_t\theta + \dfrac{2}{3\rho}\displaystyle\int_0^\infty \tilde{\theta}\,\mathrm{d}\xi = S, \\
\tilde{\theta} - \varepsilon^2\nabla_X\cdot\left(\mu\nabla_X\left(\nu\tilde{\theta}\right)\right) = -\nabla_X\cdot\left(\kappa\nabla_X\theta\right),
\end{cases}$$

We derive a numerical scheme for this problem by following the reasoning proposed for the classical Spitzer-Härm equation. It yields

$$\begin{aligned}
&\tilde{\theta}_{j,k}^{n+\tau,r+1} - \frac{\varepsilon^2}{|\mathscr{C}_k|}\sum_{f\in\mathbb{F}_{\mathscr{C}_k}} \mu_{j,f}^{n+\tau,r}\nabla_{T_f}\left[\nu_j^{n+\tau,r}\tilde{\theta}_j^{n+\tau,r+1}\right]\cdot N_{\mathscr{C}_k}^f \\
&\quad - \frac{1}{|\mathscr{C}_k|}\sum_{f\in\mathbb{F}_{\mathscr{C}_k}} \frac{2\kappa_{j,f}^{n+\tau,r}\tau h_t}{3}\nabla_{T_f}\left[\frac{1}{\rho}\sum_{l=1}^{g}\omega_l\tilde{\theta}_l^{n+\tau,r+1}\right]\cdot N_{\mathscr{C}_k}^f \\
&\qquad = -\frac{1}{|\mathscr{C}_k|}\sum_{f\in\mathbb{F}_{\mathscr{C}_k}} \kappa_{j,f}^{n+\tau,r}\nabla_{T_f}\left[\theta^n + \tau h_t S_k^{n,n+1}\right]\cdot N_{\mathscr{C}_k}^f, \\
&\theta_k^{n+\tau,r+1} = \theta_k^n + \tau h_t S_k^{n,n+1} - \frac{2\tau h_t}{3\rho_k}\sum_{j=1}^{g}\omega_j\tilde{\theta}_{j,k}^{n+\tau,r+1}.
\end{aligned} \tag{2.20}$$

On the same token, it is worthwhile showing that the scheme (2.15)-(2.16) adapts readily to treat (2.19). Since we neglect the time derivative of the generalized heat flux, we obtain

$$\begin{aligned}
&\mathcal{Q}_{j,f}^{n+\tau,r+1} - \varepsilon^2\mu_{j,f}^{n+\tau,r}\nabla_{T_f}\left[\frac{\nu_j^{n+\tau,r}}{|\mathscr{C}|}\sum_{f^\star\in\mathbb{F}_{\mathscr{C}}}\mathcal{Q}_{j,f^\star}^{n+\tau,r+1}\cdot N_{\mathscr{C}_k}^f\right] \\
&\quad - \frac{2\kappa_{j,f}^{n+\tau,r}\tau h_t}{3}\nabla_{T_f}\left[\frac{1}{\rho|\mathscr{C}|}\sum_{f^\star\in\mathbb{F}_{\mathscr{C}}}\sum_{l=1}^{g}\omega_l\mathcal{Q}_{l,f^\star}^{n+\tau,r+1}\cdot N_{\mathscr{C}_k}^f\right] \\
&\qquad = -\kappa_{j,f}^{n+\tau,r}\nabla_{T_f}\left[\theta^n + \tau h_t S_k^{n,n+1}\right], \\
&\theta_k^{n+\tau,r+1} = \theta_k^n + \tau h_t S_k^{n,n+1} - \frac{2\tau h_t}{3\rho_k|\mathscr{C}_k|}\sum_{f\in\mathbb{F}_{\mathscr{C}_k}}\sum_{j=1}^{g}\omega_j\mathcal{Q}_{j,f}^{n+\tau,r+1}\cdot N_{\mathscr{C}_k}^f.
\end{aligned} \tag{2.21}$$

We remark that (2.21) leads to (2.20) when summing the flux equations over the faces of the control volume $\mathscr{C}_k$ and defining the discrete version of the new variable $\tilde{\theta}$ as to be $\tilde{\theta}_{j,k}^{n+\tau,r+1} = \sum_{f^\star\in\mathbb{F}_{\mathscr{C}}}\mathcal{Q}_{j,f^\star}^{n+\tau,r+1}\cdot N_{\mathscr{C}_k}^f$. In practice the formulation (2.20) has to be preferred over (2.21) for simulating the Schurtz-Nicolaï model because the corresponding linear system is symmetric, and, for a given mesh, it has both a smaller size and a smaller stencil. The method adapts to more complicated delocalized operators, as presented in [3]. For instance we can introduce as a new unknown the jacobian of the generalized heat flux $\tilde{\Theta}(t,x,\xi) = \nabla_X\mathcal{Q}(t,x,\xi)$ or its discrete version $\tilde{\Theta}_{j,k}^{n+\tau,r+1} = \mathscr{G}\left[\mathcal{Q}_j^{n+\tau,r+1}\right] = \frac{1}{|\mathscr{C}_k|}\sum_{f\in\mathbb{F}_{\mathscr{C}_k}}\mathcal{Q}_{j,f}^{n+\tau,r+1}\otimes N_f$. Then the previous construction can be repeated to define a numerical scheme. However, the new variable is now a matrix and it is not clear that the resulting scheme is more effective than a version of (2.21) with a discretization of the complete delocalized operator.

3. Coupling of models: domain decomposition approach

For many applications, for instance for ICF computations and the design of devices of energy deposit by laser beams, the asymptotic Spitzer-Härm approximation is valid on a large part of the simulation domain. As discussed above, the Spitzer-Härm model is quite simple, and it can be numerically treated for a reasonable cost. However, the zones where the Spitzer-Härm model does not apply are precisely located at places where discrepancies can have a major impact on the studied physics. A simulation based

on the generalized model on the full domain is certainly unnecessarily costly. For these reasons, we explain now how we can combine the two modeling, just using the complex model where it is needed, through a coupling strategy. Since the scheme (2.15)-(2.16) is asymptotically consistent to the scheme (2.11) for the Spitzer-Härm equation, we do not need too much additional numerical tools. The discussion relies on the definition of coupling conditions and on finding a practical method to detect where the interface has to be placed. We propose an "a priori" estimator to decide where the asymptotic Spitzer-Härm equation has to be used.

3.1. Coupling strategy

Let us first suppose that the scheme is well-defined on each triangle of the mesh. We note by Ω_{SH} the part of the domain where the Spitzer-Härm model is valid and Ω_{SHG} the remainder of the computational domain. We suppose that the interface Σ between the two subdomains Ω_{SH} and Ω_{SHG} is made of a set of vertices of triangles of the primal mesh $\mathbb{T}$. Obviously, far from the interface Σ, we do not modify the models. However, close to the interface, the updating of the numerical unknowns from one subdomain depends on the values on the complementary subdomain. Hence, we need to adapt the definition of the operator $\mathscr{G}$. Remark that with the scheme (2.11), the numerical unknowns depend on their direct neighbors.

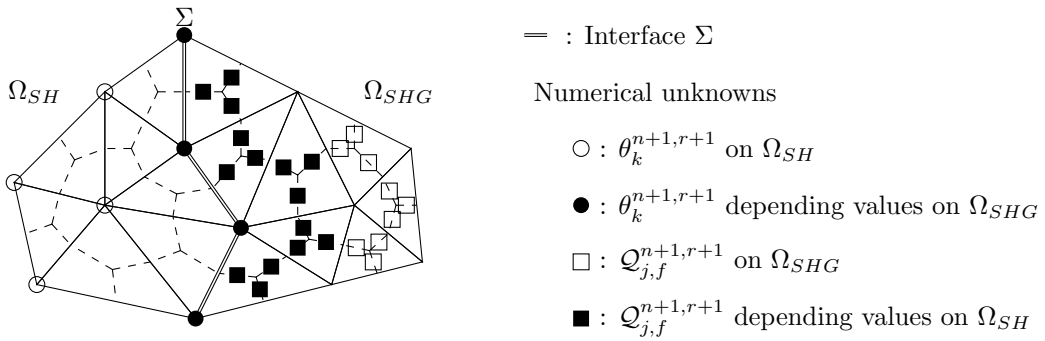

Figure 2: Numerical discretization near to the interface.

Depending whether a given volume belongs to Ω_{SH} or Ω_{SHG} we apply the scheme (2.11) or (2.15)-(2.16). We are now interested in the definition of the scheme on the interfaces. First we slightly generalize the operator $\mathscr{G}$ so that we can approach gradient on control volumes involved by the interface. We split the summation in (2.14) according to the two subdomains. Coming back to (2.18), $\mathcal{Q}_{j,f}^{n+1,r+1}$ becomes $-\kappa_{j,f}^{n+1,r+1}\nabla_{T_f}\left[\theta^{n+\tau,r+1}\right]$ in the subdomain Ω_{SH}. We define

$$\mathscr{G}_k^\star\left[\mathcal{Q}_j^{n+\tau,r+1}\right] = \frac{1}{|\mathscr{C}_k|}\Big(\sum_{f\in\mathbb{F}_{\mathscr{C}_k}\cap\Omega_{SHG}} \mathcal{Q}_{j,f}^{n+\tau,r+1}\otimes N_{\mathscr{C}_k}^f - \sum_{f\in\mathbb{F}_{\mathscr{C}_k}\cap\Omega_{SH}} \kappa_{j,f}^{n+\tau,r}\nabla_{\mathbb{T}_f}\left[\theta^{n+\tau,r+1}\right]\otimes N_{\mathscr{C}_k}^f\Big). \tag{3.1}$$

Notice that $\kappa_{j,f}^{n+\tau,r+1}$ is well defined even in the subdomain Ω_{SH} since κ depends on ξ and θ only. Then we are able to define the same operator on the hydrodynamic heat flux which appears in (2.11). Since $\mathscr{G}_k^\star$

is a linear operator, we have

$$\begin{aligned}\mathscr{G}_k^\star\left[Q^{n+\tau,r+1}\right] &= \frac{1}{|\mathscr{C}_k|}\Big(\sum_{f\in\mathbb{F}_{\mathscr{C}_k}\cap\Omega_{SHG}}\sum_{j=1}^{g}\omega_j\mathcal{Q}_{j,f}^{n+\tau,r+1}\otimes N_{\mathscr{C}_k}^f \\ &\quad - \sum_{f\in\mathbb{F}_{\mathscr{C}_k}\cap\Omega_{SH}}\kappa_{SH,f}^{n+\tau,r}\nabla_{\mathbb{T}_f}\left[\theta^{n+\tau,r+1}\right]\otimes N_{\mathscr{C}_k}^f\Big).\end{aligned} \tag{3.2}$$

The coupled scheme summarizes as follows

$$\begin{cases} \theta_k^{n+\tau,r+1}+\frac{2\tau h_t}{3\rho_k}\operatorname{Tr}\left(\mathscr{G}^\star\left[Q^{n+\tau,r+1}\right]\right)=\theta_k^n+\tau h_t S_k^{n,n+1}, & \text{for any } k\in\Omega_{SH},\\[2ex] \mathcal{Q}_{j,f}^{n+\tau,r+1}-\varepsilon^2\tilde{\mu}_{j,f}^{n+\tau,r}\nabla_{T_f}\left[\nu_j^{n+\tau,r}\operatorname{Tr}\left(\mathscr{G}^\star\left[\mathcal{Q}_j^{n+\tau,r+1}\right]\right)\right] \\ \quad -\frac{2\tilde{\kappa}_{j,f}^{n+\tau,r}\tau h_t}{3}\nabla_{T_f}\left[\frac{1}{\rho}\operatorname{Tr}\big(\mathscr{G}^\star\left[Q^{n+\tau,r+1}\right]\big)\right]-\varepsilon^2\tilde{\mu}_{j,f}^{n+\tau,r}\eta_{j,f}^{n+\tau,r}\mathcal{E}_f^{n+\tau,r+1} \\ \quad =\frac{\varepsilon^2\tilde{\mu}_{j,f}^{n+\tau,r}}{\tau h_t}\mathcal{Q}_{j,f}^n-\tilde{\kappa}_{j,f}^{n+\tau,r}\nabla_{T_f}\left[\theta^n+\tau h_t S^{n,n+1}\right], & \text{for any } f\in\Omega_{SHG}, \end{cases} \tag{3.3}$$

and furthermore

$$\theta_k^{n+\tau,r+1}=\theta_k^n+\tau h_t S_k^{n,n+1}-\frac{2\tau h_t}{3\rho_k}\operatorname{Tr}\left(\mathscr{G}^\star\left[Q^{n+\tau,r+1}\right]\right), \qquad \text{for any } k\in\Omega_{SHG}\setminus\Sigma.$$

Remark that the evaluation of the temperature on $\Omega_{SHG}\setminus\Sigma$ can be performed explicitly having at hand the quantities determined by solving the system (3.3). Reproducing the proof of Proposition 2.1. we justify the energy balance.

Proposition 3.1. *The solution of the scheme* (3.3) *satisfies the following discrete analog of* (1.7)

$$\sum_{k\in\mathbb{V}}3|\mathscr{C}_k|\rho_k\theta_k^{n+1}=\sum_{k\in\mathbb{V}}3|\mathscr{C}_k|\rho_k\theta_k^n+h_t\sum_{k\in\mathbb{V}}3|\mathscr{C}_k|\rho_k S_k^{n,n+1}.$$

3.2. "A priori" estimator

We wish now to discuss a relevant definition of the interface Σ. A rough method simply consists in splitting the domain once for all at the beginning of the simulation according to the knowledge of experimental data. The subdomain Ω_{SH} corresponds to a region where the perturbation are expected to remain small, with small variation of the temperature θ: the asymptotic Spitzer-Härm model is likely accurate enough. However, this method does not adapt to numerical results and leads to make use of a subdomain Ω_{SHG} larger than needed. A more refined method defines dynamically the subdomains by using a local estimate of the variation of the heat flux. The subdomains can be defined at each iteration or after a fixed number of time iterations, in order to keep a number of numerical unknowns as small as possible in the scheme (2.15)-(2.16).

Let us denote $\Omega_{SH}^{n,r}$ and $\Omega_{SHG}^{n,r}$ the subdomains at iteration (n,r). We know the solution $\theta^{n+\tau,r}$ on the subdomain $\Omega_{SH}^{n+1,r}$ and $\mathcal{Q}_{j,f}^{n+\tau,r}$ on the subdomain $\Omega_{SHG}^{n+1,r}$. We now construct an "a priori" estimator $E_T^{n+1,r+1}$ which will be used to update the new subdomain $\Omega_{SH}^{n+1,r+1}$ and $\Omega_{SHG}^{n+1,r+1}$. Note that since the subdomains change from one iteration to another, we shall need to define the value of $\mathcal{Q}_{j,f}^{n,r}$ in the

subdomain $\Omega_{SH}^{n+1,r} \cap \Omega_{SHG}^{n+1,r+1}$. We start by expanding the definition of the generalized heat flux to the subdomain $\Omega_{SH}^{n+1,r}$ by equating it to the asymptotic value of $\mathcal{Q}_{j,f}^{n+\tau,r}$ as ε goes to 0. Using (2.18), we write

$$\mathcal{Q}_{j,f}^{n+\tau,r} = -\kappa_{j,f}^{n+1,r-1} \nabla_{T_f} \left[\theta^{n+\tau,r}\right], \qquad \text{for any } f \in \Omega_{SH}. \tag{3.4}$$

Obviously the perturbation of the field vanishes on $\Omega_{SH}^{n+1,r}$. Since ε is not vanishing, the generalized heat flux $\mathcal{Q}_{j,f}^{n+\tau,r}$ on $\Omega_{SH}^{n+1,r}$ is not solution of (2.15). Then we compare in any triangle, the solution of the two schemes. Using (2.15), we are able to compare the solution of (2.15) to its asymptotic value given by (3.4), it yields

$$\begin{aligned}
&\left|\mathcal{Q}_{j,f}^{n+\tau,r+1} + \kappa_{j,f}^{n+\tau,r} \nabla_T \left[\theta^{n+\tau,r+1}\right]\right| \\
&\quad = \varepsilon^2 \tilde{\mu}_{j,f}^{n+\tau,r+1} \left| \frac{\mathcal{Q}_{j,f}^{n} + \kappa_{j,f}^{n+\tau,r} \nabla_T \left[\theta^{n+\tau,r+1}\right]}{\tau h_t} \right. \\
&\qquad \left. + \nabla_T \left[\nu_j^{n+\tau,r} \operatorname{Tr}\left(\mathscr{G}\left[\mathcal{Q}_j^{n+\tau,r+1}\right]\right)\right] + \eta_{j,f}^{n+\tau,r} \mathcal{E}_f^{n+\tau,r+1} \right|,
\end{aligned} \tag{3.5}$$

where we used the definition (2.6) of coefficients to compare the diffusion coefficients of the two models, i.e. $\kappa_{j,f}^{n+1,r} - \tilde{\kappa}_{j,f}^{n+1,r} = \frac{\varepsilon^2 \tilde{\mu}_{j,f}^{n+1,r} \kappa_{j,f}^{n+1,r}}{\tau h_t}$. Eventually, we define the following estimator function, $E_T^{n+1,r+1}$, stepwise constant on any triangle of the whole domain Ω,

$$\begin{aligned}
E_T^{n+1,r+1} =& \varepsilon^2 \max_{\substack{f \in T \\ j \in [\![1,g]\!]}} \tilde{\mu}_{j,f}^{n+\tau,r+1} \left| \frac{\mathcal{Q}_{j,f}^{n} + \kappa_{j,f}^{n+\tau,r} \nabla_T \left[\theta^{n+\tau,r+1}\right]}{\tau h_t} \right. \\
&\left. + \nabla_T \left[\nu_j^{n+\tau,r} \operatorname{Tr}\left(\mathscr{G}\left[\mathcal{Q}_j^{n+\tau,r+1}\right]\right)\right] + \eta_{j,f}^{n+\tau,r} \mathcal{E}_f^{n+\tau,r+1} \right|.
\end{aligned} \tag{3.6}$$

Since the generalized heat flux $\mathcal{Q}_{j,f}^{n+\tau,r}$ on $\Omega_{SH}^{n+1,r}$ obtained by using formulae (3.4) is not solution of the scheme (2.15), the equality (3.5) does not hold in the subdomain $\Omega_{SH}^{n+1,r}$. The estimator function vanishes on a triangle iff the solution of the scheme (2.15) estimated in the whole domain corresponds to the solution of the scheme (2.11).

However, we cannot use directly this definition because it depends on the unknown at iteration $(n+\tau, r+1)$, which has not yet be estimated. However, according to [3, Theorem 5.1], the solution can be expected to have some regularity. Thus, the estimator at the previous iteration $E^{n+1,r}$ is an effective approximation to define the subdomains. Eventually we fix a threshold $0 < \delta \ll 1$, and for any $T \in \mathbb{T}$ we set

$$T \in \begin{cases} \Omega_{SH}^{n+1,r+1}, & \text{if } E^{n+1,r} \leq \delta, \\ \Omega_{SHG}^{n+1,r+1}, & \text{otherwise.} \end{cases}$$

This method will be further discussed in Section 4.3.

4. Numerical Results

In this section, first we check numerically the stability and consistency properties of the scheme (2.15)-(2.16). Then we perform simulations illustrating some kinetic effects not taken into account by the Spitzer-Härm equation. For all the simulations, the linear systems are inverted using the `MUMPS` library [31].

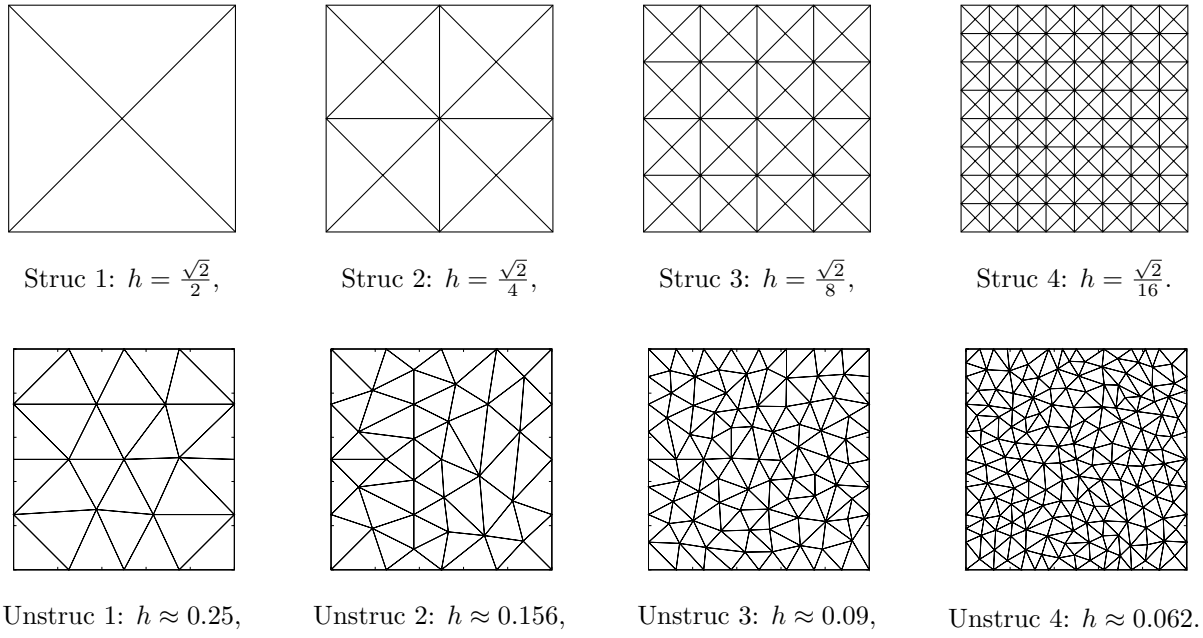

Figure 3: Examples of mesh used to estimate the consistence. In the first line, structured meshes obtained with iterative process, Struc n is the union of four Struc $n-1$ scaled by $1/2$. In the second line, unstructured meshes obtained by Delaunay triangulation using the mesh generator *Triangle*.

4.1. Validation of the Scheme

4.1.1. Consistency

In order to validate the scheme and to investigate its consistency properties we start with a simple situation where all coefficients are constants. Precisely, we set

$$\rho = \mu = \nu = \eta = 1, \qquad \kappa(\xi) = \frac{\xi^4 (\xi - 4)}{24}, \qquad \kappa_{SH} = \int_{\mathbb{R}_+} \kappa \, \mathrm{d}\xi = 1.$$

As time goes to ∞, we can expect that the solution of (1.3) tends to an asymptotic profile determined by the following system

$$\begin{cases} \displaystyle\int_\Omega \theta^\infty \, \mathrm{d}X = \int_\Omega \theta^0 \, \mathrm{d}X + \int_0^\infty \int_\Omega S \, \mathrm{d}X \, \mathrm{d}t, \\ \displaystyle\frac{2}{3\rho} \nabla_X \cdot Q^\infty = S, \\ Q^\infty - \varepsilon^2 \mu \nabla_X \left(\nu \nabla_X \cdot Q^\infty \right) = -\kappa_{SH} \nabla_X \theta^\infty, \\ \mathcal{E}^\infty = 0. \end{cases} \tag{4.1}$$

The computational domain is the square $\Omega = [0,1]^2$ and the initial condition is $\theta^0(X) = 100$ and $\mathcal{Q}_j^0(X) = 0$. We work with the following source term

$$S(x_1, x_2) = \frac{4 (2\pi)^2 \kappa_{SH}}{3\rho} \cos(2\pi x_1) \cos(2\pi x_2). \tag{4.2}$$

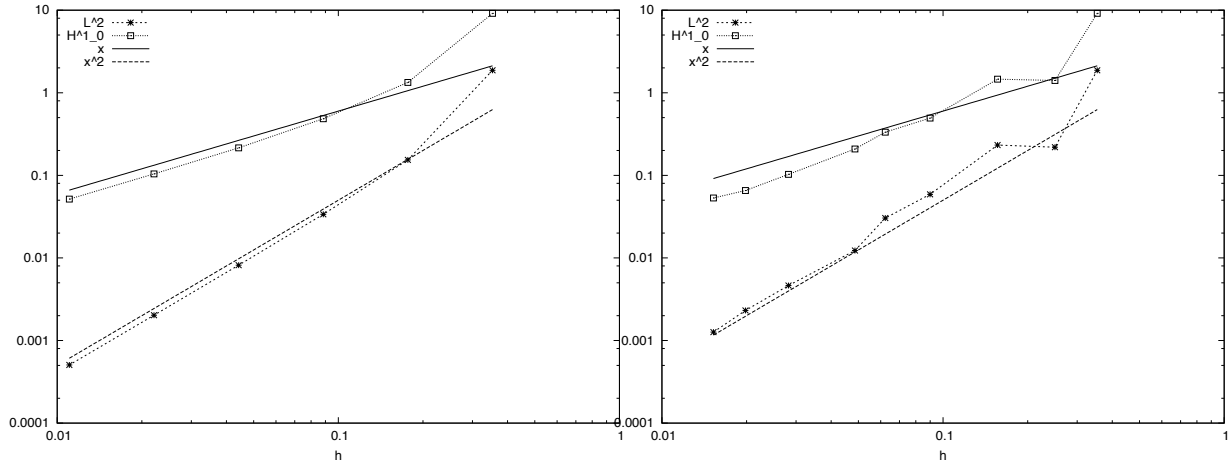

Structured meshes. Unstructured meshes.

Figure 4: Errors in the L^2 norm and in the H_0^1 norm between the numerical and the analytical results.

We can easily check that the corresponding solution of (4.1) is given by

$$\theta^{\infty}(x_1, x_2) = \int_{\Omega} \theta^0 \, \mathrm{d}X + \left(1 + 2\varepsilon^2 (2\pi)^2 \mu\nu\right) \cos(2\pi x_1) \cos(2\pi x_2).$$

We perform two sets of simulations, in a stuctured grid presented in the first line of Figure 3, and in a unstructured grid shown for some value of h, the size of the smallest edge of the mesh. We denote θ_h^{∞} the solution produced by the scheme (2.15)-(2.16) with a mesh characterized by h. We estimate the error $\theta^{\infty} - \theta_h^{\infty}$ with both the $L^2(\mathbb{T})$ norm and the $H_0^1(\mathbb{T})$ norm, the discrete norms being defined by

$$|\theta_h^n - \theta^{\infty}|_{L^2(\mathbb{T})} = \left(\sum_{\mathscr{C}_k \in \mathbb{C}} |\mathscr{C}_k| |\theta_k^n - \theta^{\infty}(X_k)|^2 \right)^{1/2}, \qquad |\theta_h^n - \theta^{\infty}|_{H_0^1(\mathbb{T})} = \left(\sum_{T \in \mathbb{T}} |T| \, |\nabla_T [\theta^n - \theta^{\infty}]|^2 \right)^{1/2}. \tag{4.3}$$

The simulations are performed using $g = 2$ points in the energy discretization with $\alpha = 3$. The time step is set to 1and we use $\tau = 1$ (fully implicit scheme) while ε is set to 10^{-1}. Figure 4 shows that the numerical scheme (2.15)-(2.16) reaches second order accuracy for the $L^2(\mathbb{T})$ norm and first order for the $H_0^1(\mathbb{T})$ norm. Further tests show that this conclusion remains unaffected by making ε vary.

4.1.2. Influence of the Energy Discretization

We now wish to investigate on numerical grounds the influence of the energy discretization, embodied into the fitting parameters α and g. We specify how the coefficients μ, ν, η, κ depend on the energy variable ξ as follows

$$\begin{aligned} \mu &= \frac{2^{3/2}\tau_1}{\rho} \xi^{3/2} \theta^{3/2}, & \nu &= \frac{2\tau_0}{3} \xi\theta \\ \kappa &= \frac{16\tau_1}{3\sqrt{\pi}} \xi^4 (\xi - 4) e^{-\xi} \theta^{5/2}, & \eta &= \frac{4\rho}{3\sqrt{\pi}} \xi^{5/2} e^{-\xi} \theta, \end{aligned} \tag{4.4}$$

where we set $\tau_0 = 200$ and $\tau_1 = 1$. These parameters can be interpreted as relaxation time respectively in the isotropic and anisotropic direction. Such expressions can be derived from the kinetic modeling dealing

g		2	3	4
N inc		36864	49152	61440
Stencil		45	75	107
α	0	101.812	103.642	103.647
	1	101.535	103.674	103.666
	2	103.766	103.729	103.708
	3	103.806	103.774	103.751
	4	103.825	103.804	103.784

Number of unknowns, stencil and L^∞ norm.

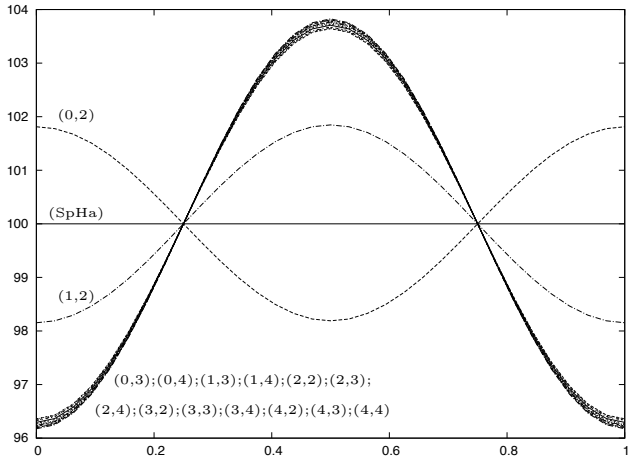

Numerical solutions on $y = 0.5$ for several value (α, g).

Figure 5: Numerical results for several value of (α, g). The left tabular is the L^∞ norm of the solution. The right figure is the temperature profile on the hyperplan $x_2 = 0.5$.

with a BGK-like collision operator, see [3]. To treat the non-linear coefficients we proceed by using the iterative procedure (2.5) until a numerical tolerance is reached; for the numerical tests the threshold is set to 10^{-10} and we do not need more than 6 iterations.

The density ρ is still assumed to be constant ($\rho(X) = 1$). The initial condition and the source term we are using are still defined by (4.2). Again we work with the structured mesh presented in Figure 3; the space step is $h = \frac{\sqrt{2}}{64}$, the time step is $h_t = 10^{-5}$ and the scheme is used in the fully implicit version $\tau = 1$. Finally we set $\varepsilon = 10^{-2}$.

Figure 5 shows the numerical results on the hyperplane $x_2 = 0.5$ for several values of g, the number of points in the energy discretization, and several value of α. The figure shows that the solution could be very bad when the number of points and the weight mismatch. For instance the results with $(\alpha, g) = (0, 2)$ are unphysical and it is worth pointing out that these parameters are violating hypothesis of [3, theorem 5.1] during the iteration process: we have at some moment $\kappa^{n,r}_{1,f} + \kappa^{n,r}_{2,f} < 0$. We also observe that the amplitude of the solution is slightly modified by the weight of the Laguerre quadrature method. The amplitude is an appropriate indicator of the impact of the non-local model. Defining the L^∞ norm of the solution by

$$|\theta^n_h|_{L^\infty(\mathbb{T})} = \max_{\mathscr{C}_k \in \mathbb{C}} \theta^n_k,$$

results are displayed at the last line of Figure 5. The convergence rate and the appropriate weight are not clearly identifiable. Thorough investigations with a larger number of points in the energy discretization are needed. However such simulations are quite expensive both in terms of CPU time and memory storage requirements. In particular, the stencil of the linear systems and thus the CPU time of the simulation increase with the number of points in the energy discretization, while they do not depend on the weight of the Laguerre polynomials. The first line in Figure 5 gives the number of punknowns of the linear system to be inverted. Obviously it is proportional to $g+1$ (generalized heat fluxes + field perturbation). The second line is the mean stencil, that is the ratio between the number of non-zero element of the linear system by

the number of lines. This result shows that the stencil increases proportionally to the number of points in the energy discretization. Then it becomes prohibitive to use a large number of quadrature points. Anyway, it seems appropriate to use parameter α which exactly estimates the asymptotic Spitzer-Härm regime with just 2 points, i.e $\alpha \in \{2, 3, 4\}$, while the parameter of delocalization ε is not too large.

4.2. Relaxation Profile and Kinetic Effect

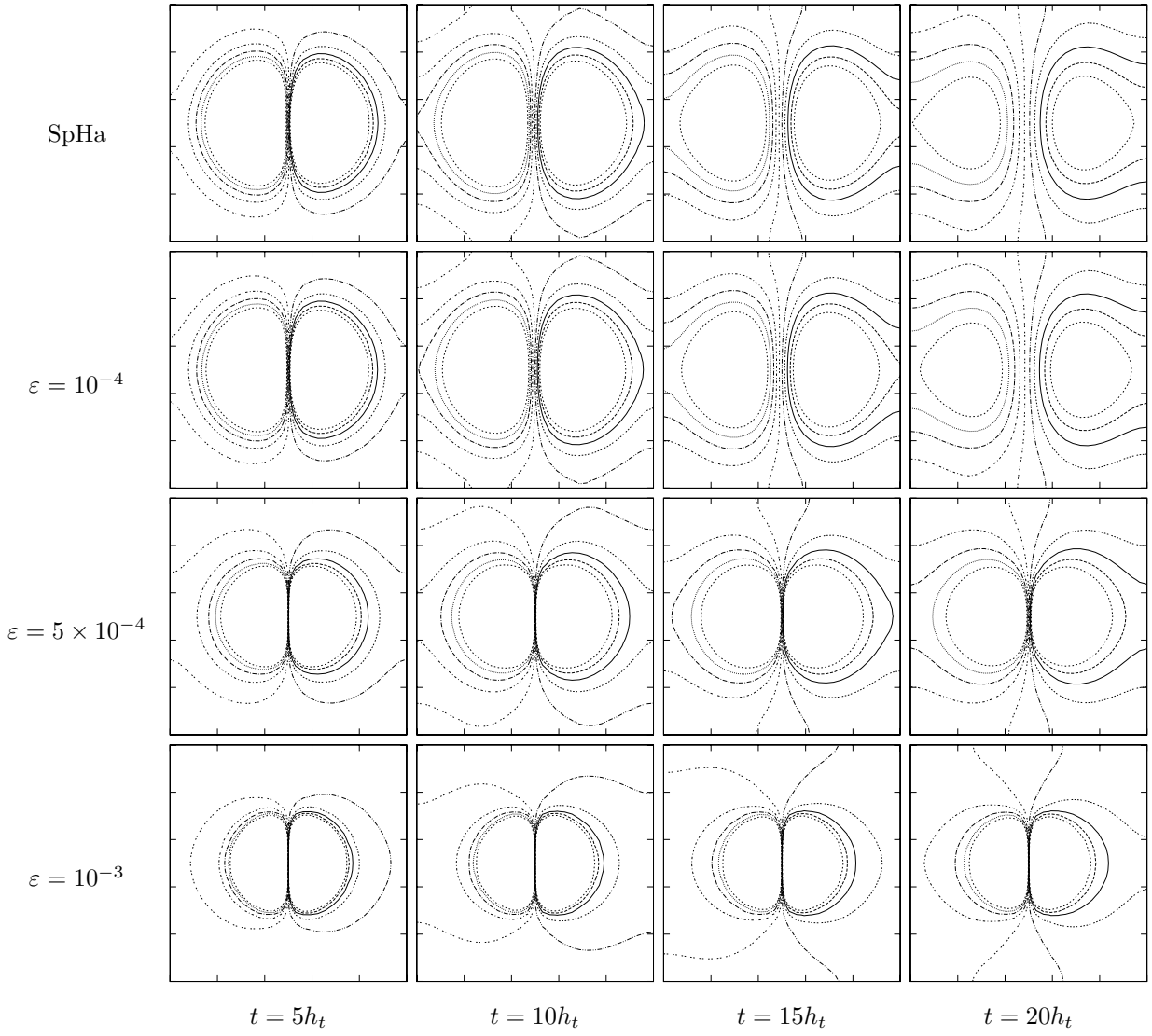

Figure 6: Temperature isoline (from 1.491 to 1.509 every 2×10^{-3}) with (2.11) (first line) and for several value of ε with (2.15)-(2.16) at some time iterations.

The following test case is closer to the simulation of plasma in practical situations. Indeed it has been

reported that the Spitzer-Härm model (1.2) is marginally valid for ICF plasmas [9]. As said above this remark has motivated the development of richer reduced models that include some delocalization effects. The relevancy of such models is evaluated by their ability in reproducing "antidiffusive effects" which are typical of the kinetic simulation: in some circumstances, the inner product between the heat flux and the temperature gradient is not necessarily negative, a feature that cannot be captured by the Spitzer-Härm equation (1.2) because $Q_{SH} \cdot \nabla_X \theta_{SH} = -\kappa_{SH} |\nabla_X \theta_{SH}|^2$ is always negative.

Hence, we consider data that produce a strong gradient initially, like

$$\theta^0(x_1, x_2) = \frac{3 + 7\cos(\pi x_1) e^{-100|X - X_c|^2}}{2}, \qquad \mathcal{Q}_j^0(X) = 0,$$

where X_c is the centroid of the computational domain. Like in the previous section, the parameters are set as follows: $\tau_0 = 200$, $\tau_1 = 1$, $\rho(X) = 1$, $h_t = 10^{-5}$, $\tau = 1$, $(\alpha, g) = (2, 2)$ and we use a structured mesh with a space step $h = \frac{\sqrt{2}}{1024}$. The tolerance for the iterative process is set to 10^{-10}. The results we discuss below are qualitatively interesting, but they should be considered with caution because on the one hand the non-linear definition of the coefficients highly depends on the physical context and they can influence the shape of the solution, and on the other hand the initialization of the heat flux we have chosen is unphysical; definitely finding relevant initial values for the $\mathcal{Q}_j$ is a difficulty when using this kind of hydrodynamic models.

Figure 6 shows the temperature contour lines for several values of ε. As ε goes to 0, the solution of (2.15)-(2.16) (first line in Figure 6) goes to the solution of (2.11) (second and fourth lines of Figure 6). For ε as small as 10^{-4}, the numerical discrepancies between the two solutions are not significant. In addition, we clearly identify that the spreading of temperature with the non local model (1.3) is reduced significantly as ε increases. This effect is more important in areas with large temperature gradients. Simulation with $\varepsilon = 5 \times 10^{-4}$ in Figure 6 illustrates this remark. When temperature gradients are smaller, the solution looks like the solution of the classical Spitzer-Härm model, yet the large gradient area ($X = .5$) is preserved. We observe that the number of iterations needed to obtain the tolerance in the iterative procedure depends on the value of the scaling parameter ε. For $\varepsilon = 0$, the maximum number of iterations increases to 11, exactly as for the Spitzer-Härm scheme (2.11) with the same iterative method to treat non linearities. As ε increases, the maximum number of iterations decreases (7 steps for $\varepsilon = 10^{-3}$). According to the intuition, more iterations are needed during the few first time steps of the simulation. In fact, the number of iterations decreases during the simulation because the evolution of the temperature becomes slower. For the last time steps and whatever the value of ε we use, the iterative procedure needs 3 iterations, which is the least number of steps imposed by the construction: the first iteration does not consider non-linearity of coefficients, and the last iteration does not modify significantly the result but is needed to perform the convergence test.

In [2, 3], simulations in one dimension have shown that (1.3) can reproduce "antidiffusive effects". Here, a difficulty comes from the fact that the numerical scheme (2.15)-(2.16) does not estimate the heat flux but rather its projection to the normal direction to the faces of the control volume (see Remark 2.1: the numerical unknown for the fluxes is actually $\mathcal{Q}_{j,f}^{n,r} \cdot N_{\mathscr{C}_k}^f$). Hence the definition of the inner product between the heat flux and temperature gradient at the discrete level is ambiguous. Therefore, we consider the following quantity, evaluated on the faces of the dual mesh

$$\langle Q_f ; \nabla_{T_f} \theta \rangle = \left(\sum_{j=1}^{g} \omega_j \mathcal{Q}_{j,f}^n \cdot N_{\mathscr{C}_k}^f \right) \left(\nabla_{T_f} \theta^n \cdot N_{\mathscr{C}_k}^f \right). \tag{4.5}$$

For the Spizer-Härm equation this quantity becomes, see (2.12), $Q_{SH,f}^n \cdot N_{\mathscr{C}_k}^f \times \nabla_t \theta_{SH}^n \cdot N_{\mathscr{C}_k}^f = -\kappa_{SH} \left(\nabla_t \theta_{SH}^n \cdot N_{\mathscr{C}_k}^f \right)^2$.

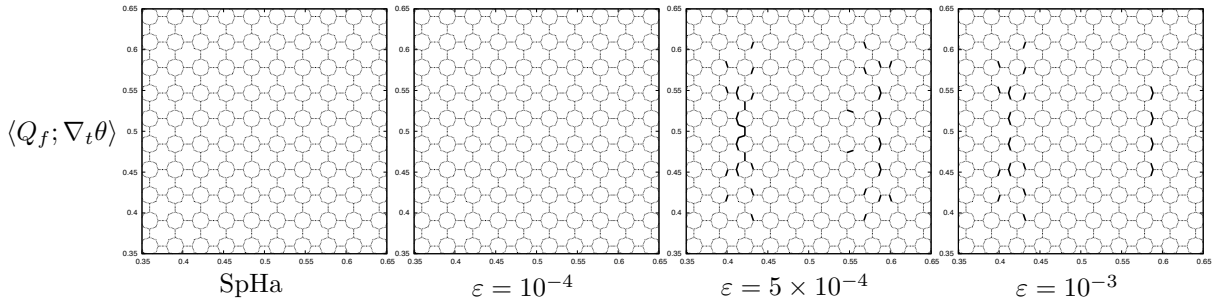

Figure 7: Product $\langle Q_f; \nabla_t \theta \rangle$ defined by (4.5) with (2.11) (first figure) and with (2.15)-(2.16) for several value of ε (second and fourth figure) zoomed on the central area at $t = 5h_t$. Dotted lines are faces with $\langle Q_f; \nabla_t \theta \rangle \leq 0$ and full lines are faces with $\langle Q_f; \nabla_t \theta \rangle > 0$.

Figure 7 shows that the product (4.5) can become positive when running (2.15)-(2.16) with $\varepsilon > 0$: on the faces marked with full lines in Figure 7 the heat flux goes in the opposite direction compared to the Spitzer-Härm flux. As expected these effects are very localized in regions of large temperature gradients. Nevertheless the impact of such effects in applications can be important because it generally occurs precisely where the main part of energy is deposited by the source (Laser Beam).

4.3. Domain decomposition impact

Let us point out that using (1.3) in the whole domain could be needlessly expensive. In view of the numerical results it is likely relevant to adopt a domain decomposition approach, using the standard Spitzer-Härm equation (1.2) in the main domain and the more involved system (1.3) in regions where large temperature gradients are observed, as it is described in Section 3.2. We remind that, for most applications we are aware of, such regions are very localized.

To illustrate the accuracy of the coupling strategy, we now perform a test case with a very localized source term. More precisely we set

$$S(x_1, x_2) = 10^7 \cos(\pi x_1)\, e^{-1000|X - X_c|^2}$$

where X_c is the centroid of the computational domain. Note that the average of the source term over the whole domain vanishes. Then we estimate the solution provided by the schemes at equilibrium. The parameters are set as follows: $\tau_0 = 200$, $\tau_1 = 1$, $\rho(X) = 1$, $\tau = 1$, $(\alpha, g) = (2, 2)$ and we use a structured mesh with a space step $h = \frac{\sqrt{2}}{512}$.

Figure 8 shows the solution of the simulation with the models (1.2) (scheme (2.11), left figure) and (1.3) (scheme (2.15)-(2.16), right figure), respectively. The diffusion of the temperature is less important for the generalized Spitzer-Härm model and the temperature remains larger in the region of the source term. Figure 9 shows the accuracy of the coupling strategy. On the left part of the figure, we plot the error in the L_2-norm and H_0^1-norm between the solutions obtained with the coupled scheme (3.3) and the solution obtained with the non-local model (2.15)-(2.16) used everywhere in the domain, for several values of the threshold parameter δ. For a small enough value of δ ($< 10^{-4}$), the coupling strategy leads exactly to the same result than the scheme (2.15)-(2.16). This has to be compared with the right part of the figure where we plot informations about the linear systems like the number of unknowns and the stencil of the coupling resolution for several values of the threshold parameter δ. Remark that for small values of δ ($< 10^{-4}$), the linear system is the same than the one of the scheme (2.15)-(2.16), and for large values of δ ($\geq 10^4$), it is the same than the one of the scheme (2.11).

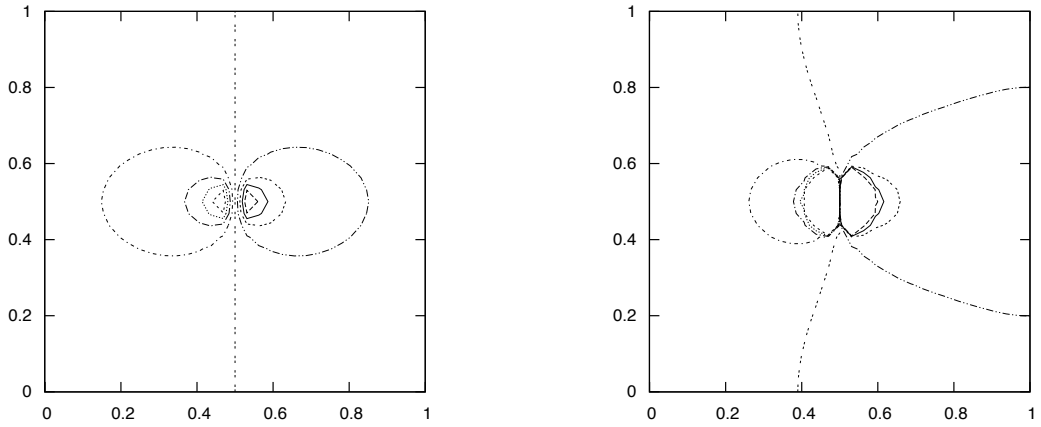

Numerical solution
of scheme (2.11).

Numerical solution
of scheme (2.15)-(2.16)

Figure 8: Isoline of the numerical solutions for the two different models (1.2) (scheme (2.11), left) and (1.3) (scheme (2.15)-(2.16), right) from 9.992 to 10.008 every 0.002.

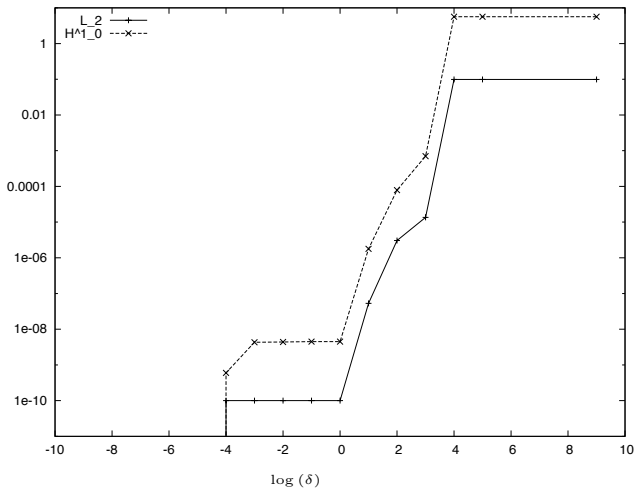

Errors in the L^2 norm and in the H_0^1 norm.

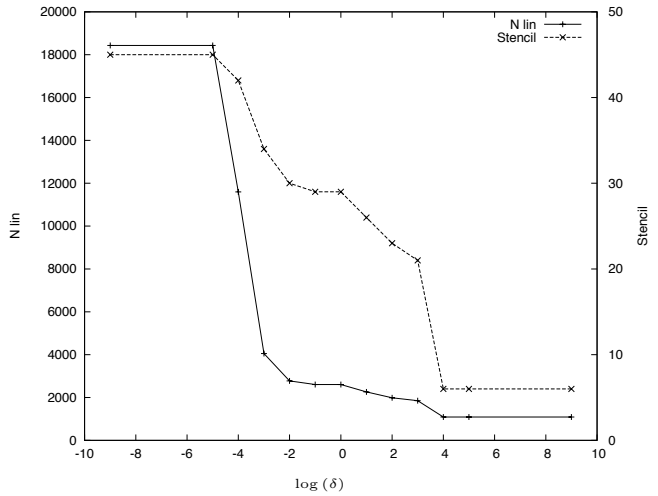

Nombre of unknowns (N lin) and mean stencil of the linear system of the scheme (3.3).

Figure 9: Comparison between the numerical results of the coupling strategy (3.3) and the scheme (2.15)-(2.16) in the whole domain.

In the intermediate range $10^{-2} \leq \delta \leq 1$, the coupling strategy leads to results quite close to the solution of (2.15)-(2.16) and the linear system is substantially smaller in number of unknowns and in stencil than when using (2.15)-(2.16). In addition, the linear system can be organized block–wise, according to the sub-domain Ω_{SH}, with symmetric blocks. This remark makes the use of parallelization strategies very appealing to solve the linear system. Eventually, note that for $10^{-4} < \delta < 10^{-2}$, the iterative process needed to estimate the non-linearity and the sub-domains converges with some difficulties. The number of iterations can grow up to several tens. It is due to the fact that the space variation of the estimator (define in (3.6)) is small in a large region where the value of the estimator is close to δ. The iterative process needs more iterations to determine the sub-domain interface and the efficiency of the strategy is limited. Figure 10 shows the sub-domain interfaces for several values of the parameter δ. For $10^{-4} \leq \delta \leq 10^{-2}$, the sub-domains are not symmetric according to the axes $y = 0.5$, as the solution needs to be. The sub-domains interfaces oscillate from close contours. For larger values of δ, these oscillations do not appear and the convergence of the iterative process is quite fast.

The example is quite specific. For real cases, it is difficult to predict how large is the domain in which heat transfer is indeed non local. It is likely that in ICF experiments the plasma evolves with non local features in a more dynamical way and in a larger region. However, this test shows that it is possible to couple the generalized model to the standard Spitzer-Härm equation, so that significant gain on the numerical cost can be obtained for a simulation made on a domain larger by several order of magnitude than the hohlraum.

5. Generalizations and Comments

5.1. Higher Dimensions and General Meshes

The scheme presented in Section 2.1.2 can be generalized to the three dimensions framework. In this context, the mesh is composed by tetrahedrons which replace the triangles used in two dimensions. The numerical unknowns corresponding to the temperature are still stored at the vertices of the mesh. The control volume of a given vertex k is the set of points in $\mathbb{R}^3$ limited by an assembly of triangular facets, where each facet is formed by connecting edge midpoints, element centroids and face centroids in the primal mesh, in such a way that only the node k is contained within the dual mesh cell, see [32]. The generalized heat fluxes are thus stored at the centroids of the faces of the volume control (hence they are 12 values per tetrahedron instead of 3 per triangle in two dimensions). Since tetrahedrons have four vertices, we can build the $\mathscr{P}$ operator as we did in two dimensions, it now defines a piecewise $\mathbb{P}_1$ function depending on the three space coordinates. Remark that the Matrix operator $\mathscr{G}$ is well defined in any dimension and for any bounded control volume. The scheme can be generalized as well to meshes made of elements more complex than triangles or tetrahedrons. Indeed the key issue relies on the construction of the $\mathscr{P}$ operator on the elements which are determined by $d + 1$ vertices and faces. When the problem becomes overdetermined, well-documented approximation techniques can be used, e. g. least squares methods or projections, see [29, 30].

5.2. Uncoupling the Generalized Heat Fluxes

The system (2.5) is macroscopic, but it is made of $(g + 1)$ coupled equations; the resolution could be expensive, especially in multi-dimensional frameworks, for cases where the heat fluxes are vectorial unknowns (see Remark 2.1). Indeed, in (2.15), the number of unknowns and the stencil of the linear system are proportional to the number of points used in the energy discretization, as it is illustrated in Figure 5. In this Section we present a decoupling strategy so that (2.15) is replaced by an iterative process, which relies on solving g uncoupled equations at each iteration. This decoupling strategy can be interpreted as a block-Jacobi method applied to the linear system (2.15), where the blocks are defined by

the index of the energy variable. In this approach, the field needs to be estimated explicitly by means of the other unknowns. To this end we multiply the equations for the heat fluxes in (2.5) by $\frac{\omega_j}{\xi_j}$ and we sum over $j \in \{1, ..., g\}$. It yields

$$\mathcal{E}^{n+\tau,r+1} = -\frac{\displaystyle\sum_{j=1}^{g}\left[\frac{\omega_j\tilde{\mu}_j^{n+\tau,r}}{\xi_j}\left(\frac{\mathcal{Q}_j^n}{\tau h_t} + \nabla_X\left(\nu_j^{n+\tau,r}\nabla_X\cdot\left(\mathcal{Q}_j^{n+\tau,r+1}\right)\right)\right)\right]}{\displaystyle\sum_{j=1}^{g}\left[\frac{\omega_j\tilde{\mu}_j^{n+\tau,r}\eta_j^{n+\tau,r}}{\xi_j}\right]}. \tag{5.1}$$

Then we replace $\mathcal{E}^{n,r+1}$ in the equation on the generalized heat fluxes in (2.5) by its expression given by (5.1). At this step, we have written a coupled system of g (generalized heat fluxes) vectorial equations, without any approximation from (2.5). In particular, the scheme satisfies exactly the constraint (2.4). Next, we approximate the generalized heat fluxes at the quadrature point j, $\mathcal{Q}_j^{n,r+1}$, by $\hat{\mathcal{Q}}_j^{n,r+1}$, within all generalized heat fluxes at other quadrature points are estimating at the known iteration in the iterative process (2.5) (same iteration number as the one used to solve non-linearities). $\hat{\mathcal{Q}}_j^{n,r+1}$ are now defined using

$$\begin{aligned}
&\hat{\mathcal{Q}}_j^{n+\tau,r+1} - \varepsilon^2\hat{\mu}_j^{n+\tau,r}\nabla_X\left(\nu_j^{n+\tau,r}\nabla_X\cdot\hat{\mathcal{Q}}_j^{n+\tau,r+1}\right) - \frac{2}{3}\tilde{\kappa}_j^{n+\tau,r}\tau h_t\nabla_X\left(\frac{1}{\rho}\nabla_X\cdot\omega_j\hat{\mathcal{Q}}_j^{n+\tau,r+1}\right)\\
&\quad= \frac{\varepsilon^2\hat{\mu}_j^{n+\tau,r}}{\tau h_t}\hat{\mathcal{Q}}_j^n - \tilde{\kappa}_j^{n,r}\nabla_X\left(\hat{\theta}^n + \tau h_t S^{n,n+1}\right) + \frac{2}{3}\tilde{\kappa}_j^{n+\tau,r}\tau h_t\nabla_X\left(\frac{1}{\rho}\nabla_X\cdot\sum_{\substack{l=1\\l\neq j}}^{g}\omega_l\hat{\mathcal{Q}}_l^{n+\tau,r}\right)\\
&\quad- \frac{\varepsilon^2\tilde{\mu}_j^{n+\tau,r}\eta_j^{n+\tau,r}}{\displaystyle\sum_{l=1}^{g}\left[\frac{\omega_l\tilde{\mu}_l^{n+\tau,r}\eta_l^{n+\tau,r}}{\xi_l}\right]}\sum_{\substack{l=1\\l\neq j}}^{g}\left[\frac{\omega_l\tilde{\mu}_l^{n+\tau,r}}{\xi_l}\left(\frac{\hat{\mathcal{Q}}_l^n}{\tau h_t} + \nabla_X\left(\nu_l^{n+\tau,r}\nabla_X\cdot\left(\hat{\mathcal{Q}}_l^{n+\tau,r}\right)\right)\right)\right]
\end{aligned} \tag{5.2}$$

where we have set

$$\hat{\mu}_j^{n,r} = \left(1 - \frac{\frac{\omega_j\tilde{\mu}_j^{n,r}\eta_j^{n,r}}{\xi_j}}{\sum_{l=1}^{g}\left[\frac{\omega_l\tilde{\mu}_l^{n,r}\eta_l^{n,r}}{\xi_l}\right]}\right)\tilde{\mu}_j^{n,r}.$$

The differential operators in (5.2) have the same structure than the differential operators in (2.5). Finally, we write the numerical scheme following the discretization introduced in (2.1.2). We write

$$\begin{aligned}
&\hat{\mathcal{Q}}_{j,f}^{n+\tau,r+1} - \varepsilon^2\hat{\mu}_{j,f}^{n+\tau,r}\nabla_{T_f}\left[\frac{\nu_j^{n+\tau,r}}{|\mathscr{C}|}\sum_{f^\star\in\mathbb{F}_{\mathscr{C}}}\hat{\mathcal{Q}}_{j,f^\star}^{n+\tau,r+1}\cdot N_{\mathscr{C}_k}^{f^\star}\right] - \frac{2}{3}\omega_j\tilde{\kappa}_{j,f}^{n+\tau,r}\tau h_t\nabla_{T_f}\left[\frac{1}{\rho|\mathscr{C}|}\sum_{f^\star\in\mathbb{F}_{\mathscr{C}}}\hat{\mathcal{Q}}_{j,f^\star}^{n+\tau,r+1}\cdot N_{\mathscr{C}_k}^{f^\star}\right]\\
&\quad= \frac{\varepsilon^2\hat{\mu}_{j,f}^{n+\tau,r}}{\tau h_t}\hat{\mathcal{Q}}_{j,f}^n - \tilde{\kappa}_{j,f}^{n+\tau,r}\nabla_{T_f}\left[\hat{\theta}^n + \tau h_t S_k^{n,n+1}\right] + \frac{2}{3}\tilde{\kappa}_{j,f}^{n+\tau,r}\tau h_t\nabla_{T_f}\left[\frac{1}{\rho|\mathscr{C}|}\sum_{f^\star\in\mathbb{F}_{\mathscr{C}}}\sum_{\substack{l=1\\l\neq j}}^{g}\omega_l\hat{\mathcal{Q}}_{l,f^\star}^{n+\tau,r}\cdot N_{\mathscr{C}_k}^{f^\star}\right]\\
&\quad- \frac{\varepsilon^2\tilde{\mu}_{j,f}^{n+\tau,r}\eta_{j,f}^{n+\tau,r}}{\displaystyle\sum_{l=1}^{g}\left[\frac{\omega_l\tilde{\mu}_{l,f}^{n+\tau,r}\eta_{l,f}^{n+\tau,r}}{\xi_l}\right]}\sum_{\substack{l=1\\l\neq j}}^{g}\left[\frac{\omega_l\tilde{\mu}_{l,f}^{n+\tau,r}}{\xi_l}\left(\frac{\hat{\mathcal{Q}}_l^n}{\tau h_t} + \nabla_{T_f}\left[\frac{\nu_j^{n+\tau,r}}{|\mathscr{C}|}\sum_{f^\star\in\mathbb{F}_{\mathscr{C}}}\hat{\mathcal{Q}}_{j,f^\star}^{n+\tau,r}\cdot N_{\mathscr{C}_k}^{f^\star}\right]\right)\right]\\
&\hat{\theta}_k^{n+\tau,r+1} = \hat{\theta}_k^n + \tau h_t S_k^{n,n+1} - \frac{2\tau h_t}{3\rho_k|\mathscr{C}_k|}\sum_{f\in\mathbb{F}_{\mathscr{C}_k}}\sum_{j=1}^{g}\omega_j\hat{\mathcal{Q}}_{j,f}^{n+\tau,r+1}\cdot N_{\mathscr{C}_k}^f,
\end{aligned} \tag{5.3}$$

with $\hat{\theta}_k^n$ an approximation of $\frac{1}{|\mathscr{C}_k|}\int_{\mathscr{C}_k}\hat{\theta}^n\,\mathrm{d}X$, $\hat{\mathcal{Q}}_{j,f}^{n+\tau,r}$ an approximation of $\frac{1}{|f|}\int_f\hat{\mathcal{Q}}_j^{n+\tau,r}\,\mathrm{d}\sigma$ and

$$\hat{\mu}_{j,f}^{n,r}=\left(1-\frac{\frac{\omega_j\tilde{\mu}_{j,f}^{n,r}\eta_{j,f}^{n,r}}{\xi_j}}{\sum_{l=1}^{g}\left[\frac{\omega_l\tilde{\mu}_{l,f}^{n,r}\eta_{l,f}^{n,r}}{\xi_l}\right]}\right)\tilde{\mu}_{j,f}^{n,r}.$$

In summary, we replace (2.15) which requires, at each iteration of fixed point, to solve implicitly one system of $g+1$ unknowns (generalized heat fluxes plus field perturbation) at each face of the control volume by (5.3) where we have to solve implicitly g (approximated generalized heat fluxes (5.2)) equations at each face of the control volume. In (5.3), the size and the stencil of the linear systems do not depend of the number of points in the energy discretization. In addition, since the computation of the heat fluxes (5.2) are totally independent, the method can be easily parallelized, the resolution using as many processors as the number of points in the energy discretization. Note that this strategy can be used in combination with the domain decomposition approach presented in 3.2, using at least one processor for the sub-domain Ω_{SH} and as many processors as the number of the energy discretization for the sub-domain Ω_{SHG}.
However, the method has some drawbacks. In particular, now the constraint (2.4) is not exactly satisfied at each iteration, even though it holds at convergence of the iterative process.

Conclusion

This paper is concerned with non-local versions of heat transfer equations arising in plasma physics. The heat flux is obtained by solving a coupled system of parabolic-like equations, constrained by a condition of vanishing current. The model we investigate generalizes the Schurtz-Nicolaï system, which is quite popular in the ICF community. In this paper, we have introduced a Vertex-Based finite volume scheme for solving the generalized non-local Spitzer-Härm equations on multidimensional unstructured grids. Numerical experiments validate the accuracy and the asymptotic consistency of the scheme, and demonstrate the possible occurrence of anti-diffusive effects. We also discuss adaptations of the method that are relevant from a practical viewpoint.

Acknowledgements. This work is partly supported by CEA/DAM. We are gratefully indebted to J.-F. Clouet and D. Deck for many fruitful discussions and their constant encouragements.

References

[1] L. Spitzer and R. Härm. Transport phenomena in a completely ionized gas. *Phys. Rev.*, 89:977–981, 1953.

[2] T. Goudon and M. Parisot. On the Spitzer-Härm regime and non-local approximations: modeling, analysis and numerical simulations. *SIAM Multiscale Model. Simul.*, 9:568–600, 2011.

[3] T. Goudon and M. Parisot. Non-local macroscopic models based on Gaussian closures for the Spitzer-Härm regime. *AIMS–KInetic and Related Models*, 3:735–766, 2011.

[4] B. K. Frolov, S. I. Krasheninnikov, R. J. Kingham, and J. Edwards. Heat flux calculation in the semi-collisionless regime for substantial temperature variations including magnetic field. *New J. Phys.*, 8: 56/1–16, 2006.

[5] P. Nicolaï, J.-L. Feugeas, and G. Schurtz. A practical nonlocal model for heat transport in magnetized laser plasmas. *Phys. Plasmas*, 13:032701+13, 2006.

[6] C. P. Ridgers, R. J. Kingham, and A. G. R. Thomas. Magnetic cavitation and the reemergence of nonlocal transport in laser plasmas. *Phys. Rev. Lett.*, 100:075003/1–4, 2008.

[7] G. Schurtz *et al.* Revisiting nonlocal electron-energy transport in inertial-fusion conditions. *Phys. Rev. Lett.*, 98:095002/1–4, 2007.

[8] A. Nishiguchi, T Yabe, M. G. Haines, M. Psimopoulos, and H. Takewaki. Convective amplification of magnetic fields in laser-produced plasmas by the Nernst effect. *Phys. Rev. Lett.*, 53:262–265, 1984.

[9] E. M. Epperlein and R. Short. A practical nonlocal model for electron heat transport in laser plasmas. *Phys. Fluids B*, 3:3092–3098, 1991.

[10] E. M. Epperlein and R. Short. Nonlocal heat transport effects on the filamentation of light in plasmas. *Phys. Fluids B*, 4:2211–2216, 1992.

[11] J.-F. Luciani, P. Mora, and J. Virmont. Nonlocal heat transport due to steep temperature gradients. *Phys. Rev. Lett.*, 51:1664–1667, 1983.

[12] J.-F. Luciani, P. Mora, and R. Pellat. Quasistatic heat front and delocalized heat flux. *Phys. Fluids*, 28:835–845, 1985.

[13] J.-F. Luciani and P. Mora. Resummation methods of the Chapman-Enskog expansion for a strongly inhomogeneous plasma. *J. Stat. Phys.*, 43:281–302, 1986.

[14] J.-F. Luciani and P. Mora. Nonlocal electron transport in laser created plasmas. *Laser Part. Beams*, 12:387–400, 1994.

[15] G. P. Schurtz, Ph.D. Nicolaï, and M. Busquet. A nonlocal electron conduction model for multidimensional radiation hydrodynamics codes. *Phys. Plasmas*, 7:4238–4250, 2000.

[16] D. Colombant and W. Manheimer. Numerical fluid solutions for nonlocal electron transport in hot plasmas: Equivalent diffusion versus nonlocal source. *J. Comput. Phys*, 229:4369–4381, 2010.

[17] B. Graille. *Modélisation de mélanges gazeux réactifs ionisés dissipatifs*. PhD thesis, Ecole Polytechnique, 2004.

[18] F. Allais, J.-P. Matte, F. Alouani-Bibi, and D. Stotler. Nonlocal electron parallel heat transport in divertor plasmas and atomic physics rates. In *29th EPS Conference on Plasma Phys. and Contr. Fusion Montreux, 17-21 June 2002*, volume 26B of *Europhysics Conference Abstracts*. European Physical Society, 2002. Ref. P-3.215.

[19] A. B. Kukushkin and K. V. Cherepanov. Evidences for and the models of fast nonlocal transport of heat in magnetic fusion devices. In *7-th Symposium "Current Trends in International Fusion Research: A Review", Washington, D.C., USA*, 2007.

[20] S. Galera, P.-H. Maire, and J. Breil. A two-dimensional unstructured cell-centered multi-material ALE scheme using VOF interface reconstruction. *J. Comput. Phys.*, 229(16):5755–5787, 2010. CODEN JCTPAH. ISSN 0021-9991. URL `http://dx.doi.org/10.1016/j.jcp.2010.04.019`.

[21] P. Hoch, S. Marchal, Y. Vasilenko, and A. A. Feiz. Non conformal adaptation and mesh smoothing for compressible Lagrangian fluid dynamics. In *CEMRACS 2007*, volume 24 of *ESAIM Proc.*, pages 111–129. EDP Sci., Les Ulis, 2008. URL `http://dx.doi.org/10.1051/proc:2008033`.

[22] G. Dujardin and P. Lafitte. Numerical analysis of the sub-cycling technique for multiscale problems. Technical report, 2012. Work in preparation.

[23] A. Hildebrandt, R. Blossey, S. Rjasanow, O. Kohlbacher, and H.-P. Lenhof. Novel formulation of nonlocal electrostatics. *Physical Review Letters*, 93, 2004. article 108104.

[24] A. Hildebrandt, R. Blossey, S. Rjasanow, O. Kohlbacher, and H.-P. Lenhof. Electrostatic potentials of proteins in water: a structured continuum approach. *Bioinformatics*, 23:e99–e103, 2007.

[25] N. Crouseilles and M. Parisot. Numerical comparison between intermediate modeling and kinetic equations. Technical report, 2012. Work in preparation.

[26] R.J. Kingham and A.R. Bell. An implicit Vlasov-Fokker-Planck code to model non-local electron transport in 2-D with magnetic fields. *J. Comput. Physics*, 194:1–34, 2004.

[27] R. Duclous, B. Dubroca, F. Filbet, and V. Tikhonchuk. High order resolution of the Maxwell-Fokker-Planck-Landau model intended for ICF applications. *J. Comput. Phys.*, 228(14):5072–5100, 2009.

[28] C. Calgaro, E. Creusé, and T. Goudon. An Hybrid Finite Volume–Finite Element method for variable density incompressible flows. *J. Comput. Phys.*, 227:4671–4696, 2008.

[29] B. Andreianov, F. Boyer, and F. Hubert. Discrete duality finite volume schemes for Leray-Lions type elliptic problems on general 2D meshes. *Numerical Methods for PDEs*, 23:145–195, 2007.

[30] Y. Coudière and F. Hubert. A 3D discrete duality finite volume method for nonlinear elliptic equations. *SIAM J. Sci. Comput.*, 33(4):1739–1764, 2011.

[31] P. Amestoy, I. Duff, and J.-Y. L'Excellent. MUMPS MUltifrontal Massively Parallel Solver version 2.0. Technical report, CERFACS, 1998.

[32] B.J. Evans, O. Hassan, J.W. Jones, K. Morgan, and L. Remaki. Simulating steady state and transient aerodynamic flows using unstructured meshes and parallel computers. *Computational Fluid Dynamic Review*, 2010:1–27, 2010.

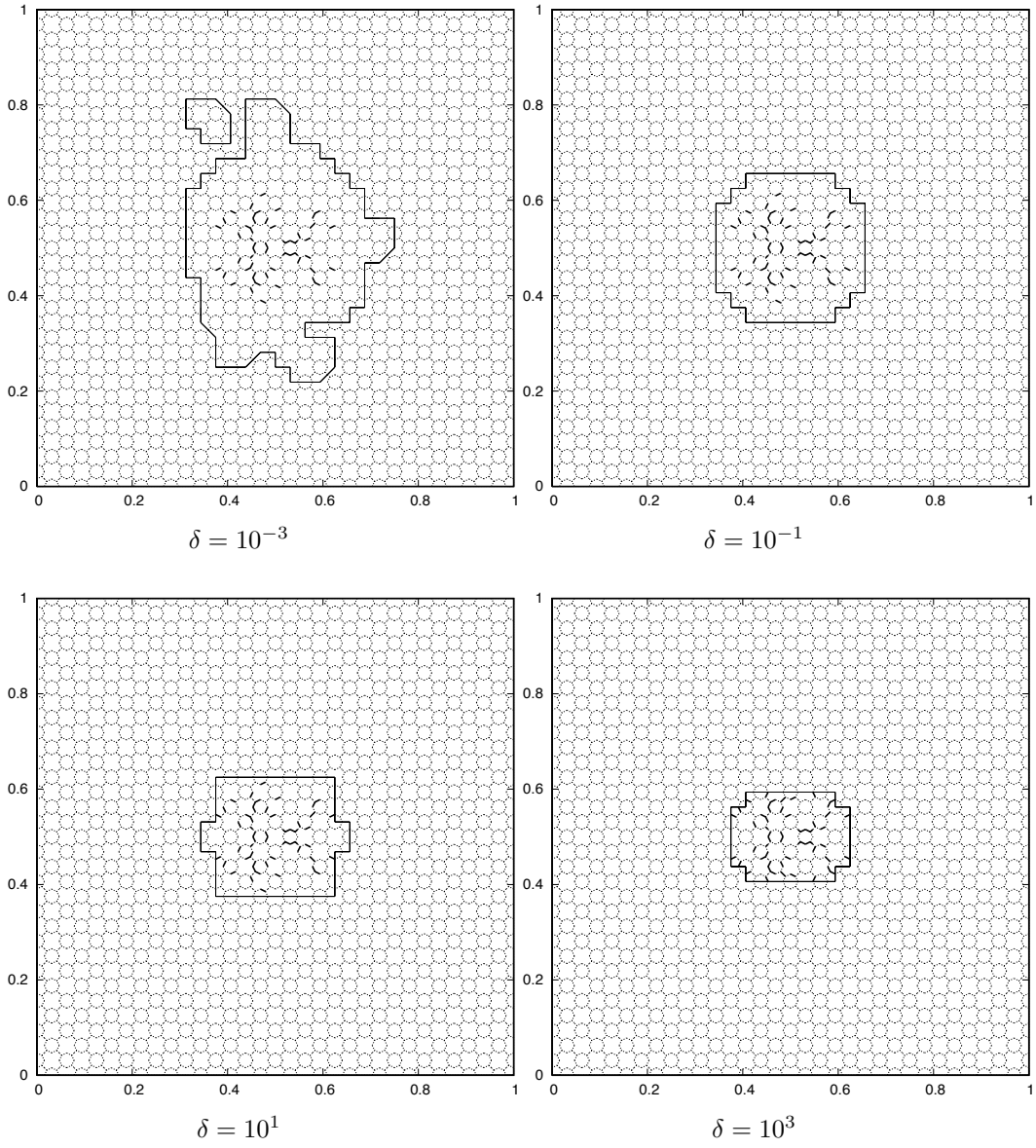

Figure 10: Product $\langle Q_f; \nabla_t \theta \rangle$ defined by (4.5) and sub-domains interface for several value of δ. Dotted lines are faces with product $\langle Q_f; \nabla_t \theta \rangle$ negative, thick plain lines are faces with product $\langle Q_f; \nabla_t \theta \rangle$ positive and thin plain lines are sub-domains interface.